SIAM J. APPL. MATH.
Vol. 83, No. 2, pp. 695–724

RESOLUTION OF 2 DIMENSIONAL RECONSTRUCTION OF FUNCTIONS WITH NONSMOOTH EDGES FROM DISCRETE RADON TRANSFORM DATA*

ALEXANDER KATSEVICH†

Abstract. Let f_ϵ, $0 < \epsilon \leq \epsilon_0$, be a family of functions in $\mathbb{R}^2$, and f_ϵ^{rec} be a reconstruction of f_ϵ from its discrete Radon transform data. Here ϵ is both the data sampling rate and the parameter of the family. We study the resolution of reconstruction when f_ϵ has a jump discontinuity along a nonsmooth curve $\mathcal{S}_\epsilon$. The assumptions are that (a) $\mathcal{S}_\epsilon$ is a family of $O(\epsilon)$-size perturbations of a smooth curve $\mathcal{S}$, and (b) $\mathcal{S}_\epsilon$ is Hölder continuous with some exponent $\gamma \in (0, 1]$. Thus the size of the perturbation $\mathcal{S} \to \mathcal{S}_\epsilon$ is of the same order of magnitude as the data sampling rate. We compute the discrete transition behavior (DTB) defined as the limit $\text{DTB}(\check{x}) := \lim_{\epsilon \to 0} f_\epsilon^{\text{rec}}(x_0 + \epsilon\check{x})$, where x_0 is generic. We illustrate the DTB by two sets of numerical experiments. In the first set, the perturbation is a smooth, rapidly oscillating sinusoid, and in the second, a fractal curve. The experiments reveal that the match between the DTB and reconstruction is worse as $\mathcal{S}_\epsilon$ gets rougher. This is in agreement with the proof of the DTB, which suggests that the rate of convergence to the limit is $O(\epsilon^{\gamma/2})$. We then propose a new DTB, which exhibits an excellent agreement with reconstructions. Investigation of this phenomenon requires computing the rate of convergence for the new DTB. This, in turn, requires completely new approaches. We obtain a partial result along these lines and formulate a conjecture that the rate of convergence of the new DTB is $O(\epsilon^{1/2} \ln(1/\epsilon))$.

Key words. Radon inversion, resolution, fractals, discrete data

MSC codes. 44A12, 65R10, 94A12

DOI. 10.1137/21M1466712

1. Introduction.

Action of the Radon transform (and, by extension, its inverse) on distributions is a topic that has received considerable attention over the years [12, 16, 37]. From a practical perspective, if an object represented by an unknown function f has singularities (e.g., jumps or edges), it is important to know how well (e.g., with what resolution) these singularities can be reconstructed when the data are discrete. Convergence of numerical Radon inversion algorithms for nonsmooth functions has been studied as well [13, 32, 34, 35]. In these works the discontinuities of the object are a complicating factor rather than the object of study.

Let $\mathcal{S}$ denote the singular support of f. Let $\check{f}$ be a reconstruction from continuous data, and $\check{f}_\epsilon$, the corresponding reconstruction from discrete data, where ϵ represents the data sampling rate. In the latter case, interpolated discrete data are substituted into the "continuous" inversion formula. When theoretically exact reconstruction is desired, $\check{f} \equiv f$. Generally, $\check{f}$ does not coincide with f. For example, one can be interested in edge-enhanced reconstruction, as in local tomography [11, 37] or when computing derivatives of f directly from the data [15, 26]. In other cases, e.g., for more general Radon transforms, an exact inversion formula may not exist. In this case one usually reconstructs f modulo less singular terms, i.e., $f - \check{f}$ is smoother than f.

In [18, 19, 20, 21, 22] the author developed the analysis of reconstruction, called *local resolution analysis*, by focusing specifically on the behavior of $\check{f}_\epsilon$ near $\mathcal{S}$. One of

* Received by the editors December 20, 2021; accepted for publication (in revised form) January 3, 2023; published electronically April 28, 2023.
https://doi.org/10.1137/21M1466712
Funding: This work was supported in part by NSF grant DMS-1906361.

† Department of Mathematics, University of Central Florida, Orlando, FL 32816-1364 USA (alexander.katsevich@ucf.edu).

the main results of these papers is the computation of the limit

$$\mathrm{DTB}(\check{x}) := \lim_{\epsilon \to 0} \epsilon^{\kappa} \check{f}_{\epsilon}(x_0 + \epsilon \check{x}) \tag{1.1}$$

in a variety of settings. Here $x_0 \in \mathcal{S}$ is generic (see Definition 2.4 below), $\kappa \geq 0$ is selected based on the strength of the singularity of $\check{f}$ at x_0, and $\check{x}$ is confined to a bounded set (e.g., to some bounded disk centered at the origin). It is important to emphasize that both the size of the neighborhood around x_0 and the data sampling rate go to zero simultaneously in (1.1). The limiting function $\mathrm{DTB}(\check{x})$, which we call the discrete transition behavior (DTB for short), contains complete information about the resolution of reconstruction. Formula (1.1) is written for a fixed x_0, which is omitted from the left-hand side for brevity. In a similar fashion, in what follows we omit the dependence of the DTB on the base point x_0. The geometric meaning of $\check{x}$ is the rescaled difference between a reconstruction point x and the base point x_0: $\check{x} = (x - x_0)/\epsilon$.

The practical use of the DTB is based on the relation

$$\check{f}_{\epsilon}(x_0 + \epsilon \check{x}) = \epsilon^{-\kappa} \mathrm{DTB}(\check{x}) + \text{error term}. \tag{1.2}$$

When $\epsilon > 0$ is sufficiently small, the error term is negligible, and $\epsilon^{-\kappa}\mathrm{DTB}(\check{x})$, which is typically computed by a simple formula, is an accurate approximation to the numerical reconstruction.

The functions, which have been investigated in the framework of local resolution analysis so far, are conormal distributions, whose wave front set coincides with the conormal bundle of a smooth surface. To put it another way, these distributions are nonsmooth across a smooth surface, and are smooth along it. On the other hand, in many applications the discontinuities of a sample f occur across nonsmooth (rough) surfaces. Examples include soil and rock imaging, where the surface of cracks and pores is highly irregular and frequently simulated by fractals [2, 14, 25, 31, 36, 38, 44].

Micro-CT (i.e., CT capable of achieving micrometer resolution) is an important tool for imaging of rock samples extracted from the well. As stated in [44], "The simulation of various rock properties based on three-dimensional digital cores plays an increasingly important role in oil and gas exploration and development. The accuracy of 3D digital core reconstruction is important for determining rock properties." Here the term "digital core" refers to a digital representation of a rock sample obtained, for example, as a result of its CT or micro-CT scanning and reconstruction. Accurate identification of the pore space inside rock samples is of utmost importance because it contributes to accurate estimation of the amount of hydrocarbon reserves in a given formation and brings many additional benefits. As stated above, the boundary between the solid matrix and the pore space is typically rough (see also [7]), i.e., it contains features across a wide range of scales, including the scales below what is accessible with micro-CT. Therefore effects that degrade the resolution of micro-CT (e.g., the partial volume effect due to finite data sampling) and how these effects manifest themselves in the presence of rough boundaries require careful investigation. Once fully understood and quantified, these effects can be accounted for to improve pore space determination when analyzing reconstructed images.

Very little is known about how the Radon transform acts on distributions with more complicated singularities. A recent literature search reveals a small number of works, which investigate the Radon transform acting on random fields [17, 40, 27]. For example, the author did not find any publication on the Radon transform of

characteristic functions of domains with rough boundaries. This appears to be the first paper on the Radon transform of functions with rough edges.

In this paper we use local resolution analysis in $\mathbb{R}^2$ to study the resolution of reconstruction for a family of functions $f_\epsilon^{\rm mod}$, which have a jump discontinuity across a nonsmooth curve. Exact reconstruction from the classical Radon transform data is considered (hence $\kappa = 0$ in (1.1)).

To construct $f_\epsilon^{\rm mod}$, we start with a piecewise C^2 function f, which has a jump discontinuity across a smooth curve $\mathcal{S}$. Let $\mathcal{S}_\epsilon$ be a family of curves, which are small perturbations of $\mathcal{S}$. The assumption is that $\mathcal{S}_\epsilon$ is Hölder continuous with some exponent $\gamma \in (0,1]$ for all $\epsilon > 0$ sufficiently small. The perturbation is of size $\delta = O(\epsilon)$, and the perturbation scales like $O(\epsilon^{-1/2})$ along $\mathcal{S}$ (see the paragraph following (2.8)). By the size of the perturbation δ we mean the maximum of $\mathrm{dist}(x, \mathcal{S}_\epsilon)$ over $x \in \mathcal{S}$. Then $f_\epsilon^{\rm mod}$ is obtained by smoothly extending the values of f on either side of $\mathcal{S}$ up to the new curve $\mathcal{S}_\epsilon$.

In practice, our assumptions mean that (1) the data sampling rate $\epsilon > 0$ is sufficiently small, but finite (similarly to (1.2)); (2) the size of the perturbation δ is comparable with or less than the data sampling rate (i.e., $\delta \lesssim \epsilon$); and (3) the oscillations in $\mathcal{S}_\epsilon$ scale like $O(\epsilon^{-1/2})$ along $\mathcal{S}$. The assumptions about $\mathcal{S}_\epsilon$ are quite reasonable. On one hand, they cover the cases $\delta \sim \epsilon$ and $\delta \ll \epsilon$. On the other hand, if $\delta \gg \epsilon$, $\mathcal{S}_\epsilon$ oscillates slowly, and $\mathcal{S}_\epsilon$ is sufficiently smooth, then we are essentially in the situation addressed in [18, 19, 20, 21, 22]. In the remaining cases, $\delta \gg \epsilon$, and either $\mathcal{S}_\epsilon$ oscillates sufficiently fast or $\mathcal{S}_\epsilon$ is sufficiently rough (or both). These are especially challenging cases, they are not covered by the existing theory, and require a separate analysis. When applying our results in practice, the main objects are $f_\epsilon^{\rm mod}$ and $\mathcal{S}_\epsilon$. The existence of f and $\mathcal{S}$ is required only for theoretical analysis.

Due to the linearity of the Radon transform, we can consider $f_\epsilon := f - f_\epsilon^{\rm mod}$, which is supported in the narrow domain bounded by $\mathcal{S}$ and $\mathcal{S}_\epsilon$ (see (2.9), Figure 1, and the paragraph preceding (2.10) below). The reconstruction of $f_\epsilon(x)$ from discrete data is denoted $f_\epsilon^{\rm rec}(x)$. We obtain the DTB by computing the limit of the kind (1.1) (with $\kappa = 0$ and $\check{f}_\epsilon$ replaced by $f_\epsilon^{\rm rec}$) and illustrate it by two sets of numerical experiments. In the first set, the perturbation $\mathcal{S} \to \mathcal{S}_\epsilon$ is a smooth sinusoid with amplitude $O(\epsilon)$ and period $O(\epsilon^{1/2})$. Results of these experiments with $\epsilon = \epsilon_1 = 1.2/500$ and $\epsilon = \epsilon_2 = 1.2/1000$ demonstrate a good agreement between the DTB and reconstruction.

The second set involves a fractal perturbation, which is specified in terms of the Weiertsrass–Mandlebrot function [4, 6]. As before, the magnitude of the perturbation is $O(\epsilon)$, and it scales like $O(\epsilon^{1/2})$ along $\mathcal{S}$. Its Hölder exponent is $\gamma = 1/2$. It turns out that the match between the DTB and reconstruction is now much worse than before for the same two values $\epsilon = \epsilon_{1,2}$. Note that the DTB is an accurate approximation to the reconstruction only when $\epsilon > 0$ is sufficiently small. Analysis of the derivation

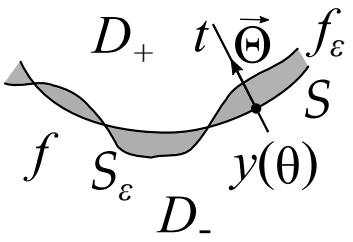

FIG. 1. *Illustration of the perturbation $\mathcal{S} \to \mathcal{S}_\epsilon$ and the function f_ϵ, which is supported in the shaded region.*

of the DTB suggests (but not proves) that the rate of convergence in (1.1) is $O(\epsilon^{\gamma/2})$ (which is also the magnitude of the error term in (1.2)). In other words, the rougher $\mathcal{S}_\epsilon$ is, the slower the convergence and the larger the error. Therefore, to obtain a good match when $\mathcal{S}_\epsilon$ is fractal, a much smaller value $\epsilon \ll \epsilon_2$ should be used.

Analysis of the reconstruction formula reveals a potentially more accurate expression for $f_\epsilon^{\text{rec}}(x_0+\epsilon\check{x})$. Even though the DTB was originally defined as the limit in (1.1), with a slight abuse of notation, any easily computable approximation to $f_\epsilon^{\text{rec}}(x_0+\epsilon\check{x})$ will be called a DTB as well and denoted DTB_{new}. In particular, DTB_{new} may have a more complicated ϵ-dependence than the one in (1.1):

$$f_\epsilon^{\text{rec}}(x_0+\epsilon\check{x}) = \text{DTB}_{\text{new}}(\check{x},\epsilon) + \text{error term}. \tag{1.3}$$

The idea is that by allowing a more general ϵ-dependence, the error term in (1.3) can be smaller than the one in (1.2).

Numerical experiments with the new DTB show a perfect match between DTB_{new} and reconstruction for the two values $\epsilon = \epsilon_{1,2}$ used before. The two results do not contradict each other, because the original, less accurate DTB is a small-ϵ limit of the new, more accurate DTB (see (7.4)–(7.6)).

Rigorous derivation of DTB_{new} is significantly more difficult than that of the original one. Even the proof of the original DTB (1.1) (see sections 3–5) establishes the existence of convergence, but not its rate (see the last paragraph in subsection 3.1). To prove that DTB_{new} is indeed more accurate, one needs to estimate its approximation error (and that of the original DTB). We distinguish two cases: $x_0 \in \mathcal{S}$ and $x_0 \notin \mathcal{S}$, and prove that in the second case, assuming in addition that there is no line through x_0 which is tangent to $\mathcal{S}$, the rate of convergence of DTB_{new} is $O(\epsilon^{1/2}\ln(1/\epsilon))$. Based on this result and numerical evidence, we formulate the conjecture that the same rate holds in the remaining, unproven cases. Our proof of the second case uses different tools and, at its core, uses a phenomenon different from the one in the proof of the original DTB. The proof of the remaining cases is difficult, requires entirely new approaches, and is outside the scope of this paper.

The new DTB (see. (7.3) below) is given by a convolution of an explicitly computed and suitably scaled kernel with f_ϵ. Thus, it can be used quite easily to investigate partial volume effects and resolution in the case of rough (e.g., fractal) boundaries. Superficially, this kernel resembles the point spread function (PSF) of filtered backprojection reconstruction [9, section 12.3]. Nevertheless, its origin, use (analysis of reconstruction in a neighborhood of a singularity of f_ϵ), and method of proof are all completely different from those for the PSF.

To summarize, the main results of the paper are as follows:

1. Derivation of the original DTB for a family of functions f_ϵ with a rough edge $\mathcal{S}_\epsilon$;
2. numerical demonstration that the accuracy of the original DTB drops as the curve $\mathcal{S}_\epsilon$, across which f_ϵ is discontinuous, becomes less smooth (fractal);
3. a new DTB is proposed, which is shown numerically to be much more accurate than the original one for fractal $\mathcal{S}_\epsilon$; and
4. a conjecture about the accuracy of the new DTB and its proof in the case $x_0 \notin \mathcal{S}$ under some additional assumptions.

Sampling theory is an alternative approach to investigate the resolution of tomographic reconstruction when f is bandlimited. Applications of the sampling theory to the classical Radon transform are in papers such as [29, 33, 10]. Sampling for distributions with semiclassical singularities is developed in [41, 28]. The goals of these

approaches are to determine the sampling rate required to reliably recover features of a given size and to describe aliasing artifacts if the sampling requirements are violated. Thus, the problem settings and the types of results obtained using sampling theory are different from those of the local resolution analysis.

The paper is organized as follows. In section 2, we describe the problem setup, state the relevant result from our earlier paper [18] as Theorem 2.5, and formulate the first result of this paper—a formula for the original DTB (1.1)—as Theorem 2.6. Section 3 contains most of the proof of the theorem. In section 4 we compute the original DTB explicitly and consider two theoretical examples. In the first one the perturbation is a constant function along $\mathcal{S}$, and we recover the result of [18]. In the second example we consider a fractal perturbation specified in terms of a Weiertsrass–Mandlebrot function. The fact that the perturbed boundary $\mathcal{S}_\epsilon$ does not create nonlocal artifacts is proven in section 5, thereby finishing the proof of Theorem 2.6. Numerical experiments with the original DTB are in section 6, where oscillatory and fractal perturbations of $\mathcal{S}$ are considered. In section 7 we describe $\mathrm{DTB}_{\mathrm{new}}$ and present numerical experiments with the new formula. The experiments demonstrate improved accuracy for fractal $\mathcal{S}_\epsilon$. We formulate a conjecture about the accuracy of $\mathrm{DTB}_{\mathrm{new}}$, and state Lemma 7.1 about the magnitude of error when $x_0 \notin \mathcal{S}$. The proof of the lemma is in Appendix C. Let $H_0(s)$ be the function that describes the perturbation $\mathcal{S} \to \mathcal{S}_\epsilon$ (after appropriate rescaling, see (2.8)). The additional assumption in Lemma 7.1 (compared with Theorem 2.6) is that the level sets of H_0, i.e., the sets $H_0^{-1}(\hat{t})$, are not too dense for almost all $\hat{t} \in H_0(\mathbb{R})$. In Appendix D we construct a function on $\mathbb{R}$, whose level sets are not too dense as required for the lemma, which is Hölder continuous with exponent γ for any prescribed $0 < \gamma < 1$, but which is not Hölder continuous with any exponent $\gamma' > \gamma$ on a dense subset of $\mathbb{R}$. Another example is the Cantor staircase function [24], which also satisfies all the assumptions, is described at the end of section 7. The proofs of two auxiliary lemmas are in Appendices A and B.

2. Preliminaries. Consider a compactly supported function $f(x)$ on the plane, $x \in \mathbb{R}^2$. Set $\mathcal{S} := \{x \in \mathbb{R}^2 : f \notin C^2(U) \text{ for any open } U \ni x\}$. Obviously, $\mathcal{S}$ is a closed set.

Assumptions 2.1 (function f).

f1. For each $x_0 \in \mathcal{S}$, which is not an endpoint of $\mathcal{S}$, there exist a neighborhood $U \ni x_0$, open sets $D_\pm$, and functions $f_\pm \in C^2(\mathbb{R}^2)$ such that

$$\begin{aligned} &f(x) = \chi_{D_-}(x) f_-(x) + \chi_{D_+}(x) f_+(x),\ x \in U \setminus \mathcal{S}, \\ &D_- \cap D_+ = \varnothing,\ D_- \cup D_+ = U \setminus \mathcal{S}, \end{aligned} \tag{2.1}$$

where $\chi_{D_\pm}$ are the characteristic functions of $D_\pm$,

f2. For each $x_0 \in \mathcal{S}$ there exists a neighborhood $U \ni x_0$ such that $\mathcal{S} \cap U$ is a C^4 curve with nonzero curvature at every point.

Assumption 2.1.f2 implies that the curve $\mathcal{S}$ is a union of finitely many sufficiently smooth, convex segments. By assumption 2.1.f1, locally $f(x) \equiv f_-(x)$ on one side of $\mathcal{S}$ ($x \in D_-$), and $f(x) \equiv f_+(x)$, on the other side ($x \in D_+$). In general, $f_-(x) \neq f_+(x)$, $x \in \mathcal{S}$, so f may have a discontinuity across $\mathcal{S}$. Since we require that $f_\pm \in C^2(\mathbb{R}^2)$, $f_-(x)$ and $f_+(x)$ are well-defined for $x \in D_+$ and $x \in D_-$, respectively.

The discrete tomographic data are given by

$$\hat{f}_\epsilon(\alpha_k, p_j) := \frac{1}{\epsilon} \iint w\left(\frac{p_j - \vec{\alpha}_k \cdot y}{\epsilon}\right) f(y) \mathrm{d}y,\ p_j = \bar{p} + j\Delta p,\ \alpha_k = \bar{\alpha} + k\Delta\alpha, \tag{2.2}$$

where w is a detector aperture function, $\Delta p = \epsilon$, $\Delta\alpha = \kappa\epsilon$, and $\kappa > 0$, $\bar{p}$, $\bar{\alpha}$, are fixed. Here and below, $\vec{\alpha}$ and α in the same equation are always related by $\vec{\alpha} = (\cos\alpha, \sin\alpha)$. The same applies to $\vec{\Theta} = (\cos\theta, \sin\theta)$ and θ.

Assumptions 2.2 (aperture function w).

AF1. w is even and $w \in C_0^2(\mathbb{R})$ (i.e., w is compactly supported, and $w'' \in L^\infty(\mathbb{R})$); and

AF2. $\int w(p)dp = 1$.

Hence, the data (2.2) represent the integrals of f along thin strips, and their width ($= O(\epsilon)$) is determined by ϵ and the support of w. This is in contrast with the ideal case, where w is the Dirac δ-function, and the data represent line integrals of f.

Reconstruction from discrete data is achieved by the formula

$$f_\epsilon^{\mathrm{rec}}(x) = -\frac{\Delta\alpha}{2\pi} \sum_{|\alpha_k| \le \pi/2} \frac{1}{\pi} \int \frac{\partial_p \sum_j \varphi\left(\frac{p-p_j}{\epsilon}\right) \hat{f}_\epsilon(\alpha_k, p_j)}{p - \alpha_k \cdot x} \mathrm{d}p, \tag{2.3}$$

where φ is an interpolation kernel. This is a discretized version of the classical filtered backprojection inversion formula for the Radon transform in $\mathbb{R}^2$ [30]). The integral with respect to p, which is understood in the principal value sense, is the filtering step (the Hilbert transform), while the external sum is a quadrature rule corresponding to the backprojection integral.

Assumptions 2.3 (interpolation kernel φ).

IK1. φ is even and $\varphi \in C_0^2(\mathbb{R})$;

IK2. φ is exact up to order 1, i.e.

$$\sum_{j \in \mathbb{Z}} j^m \varphi(u - j) \equiv u^m, \ m = 0, 1, \ u \in \mathbb{R}. \tag{2.4}$$

As is easily seen, assumption 2.3.IK2 implies $\int \varphi(p)dp = 1$.

Definition 2.4 (see [18]). *A point $x_0 \in \mathbb{R}^2$ is generic if*

1. *No line through x_0 is tangent to $\mathcal{S}$ at a point where the curvature of $\mathcal{S}$ is zero.*
2. *If $x_0 \in \mathcal{S}$, the quantity $\kappa x_0 \cdot \vec{\tau}$ is irrational, where $\vec{\tau}$ is a unit tangent vector to $\mathcal{S}$ at x_0.*

Our definition includes condition 1, because in [18] $\mathcal{S}$ is allowed to have zero curvature at isolated points. Here we assume that the curvature of $\mathcal{S}$ is nonzero at every point (Assumption 2.1.f2), so condition 1 is satisfied automatically. Consider the function $p(\alpha) = \vec{\alpha} \cdot x_0$, whose graph is a curve in the Radon space. Let α_0 be a value such that the line $\{x \in \mathbb{R}^2 : \vec{\alpha}_0 \cdot x = p(\alpha_0)\}$ is tangent to $\mathcal{S}$ at x_0. As is easily seen, $|\kappa x_0 \cdot \vec{\tau}| = (\Delta\alpha/\Delta p)|\mathrm{d}p(\alpha = \alpha_0)/\mathrm{d}\alpha|$. Hence, this quantity is dimensionless. Condition 2 says that $p(\alpha)$ has an irrational slope at $\alpha = \alpha_0$ if the scales along the p- and α-axes are Δp and $\Delta\alpha$, respectively (see (2.2)).

Pick a generic point $x_0 \in \mathcal{S}$. Let $\vec{\Theta}_0$ be the unit normal to $\mathcal{S}$ at x_0, which points from x_0 towards the center of curvature of $\mathcal{S}$ at x_0. We will call the side of $\mathcal{S}$ where $\vec{\Theta}_0$ points "positive," and the opposite side, "negative." Without loss of generality, we can assume in (2.1) that D_+ is on the positive side of $\mathcal{S}$, and D_- is on the negative side. We formulate here the relevant result from [18] (a more general result is established in [20]).

THEOREM 2.5 ([18, 20]). *Let* (a) f *satisfy Assumptions* 2.1*;* (b) *detector aperture function* w *satisfy Assumptions* 2.2*; and* (c) *interpolation kernel* φ *satisfy Assumptions* 2.3. *Suppose* $x_0 \in \mathcal{S}$ *is generic, and let* $\vec{\Theta}_0$ *be the positive unit normal to* $\mathcal{S}$ *at* x_0. *If* f_ϵ^{orig} *is the reconstruction of the original, unperturbed* f *from the data* (2.2) *using* (2.3)*, then*

$$\lim_{\epsilon\to 0} f_\epsilon^{\text{orig}}(x_0+\epsilon\check{x}) = \text{const} + (f_+(x_0) - f_-(x_0)) \int_{-\infty}^{\vec{\Theta}_0\cdot\check{x}} (\varphi * w)(r)dr, \tag{2.5}$$

where $f_\pm(x_0)$ *are the same as in* (2.1). *If* $x_0 \notin \mathcal{S}$ *is generic, then*

$$\lim_{\epsilon\to 0} f_\epsilon^{\text{orig}}(x_0+\epsilon\check{x}) = \text{const}. \tag{2.6}$$

The constants on the right in (2.5), (2.6) *may depend on* x_0*, but they are independent of* $\check{x}$.

Note that the goal of local resolution analysis is to study the resolution of reconstruction of singularities of f. Any component of the reconstruction, which is locally constant in the limit as $\epsilon \to 0$, is not relevant for our approach and is absorbed by the constants in (2.5), (2.6).

The result in [18] is formulated in the ideal case with w equal to the δ-function. In [20, section 6] it is described how to account for a finite detector aperture. Hence the above theorem is stated with w, which satisfies Assumptions 2.2.

Now we describe a family of perturbations $\mathcal{S} \to \mathcal{S}_\epsilon$. Pick any small open set U such that $\mathcal{S} \cap U$ is a single, short curve segment. Suppose $\mathcal{S} \cap U$ is parametrized by $I \ni \theta \to y(\theta) \in \mathcal{S} \cap U$ for some interval I. Here $y \in C^4(I)$, and $y(\theta)$ is the point where the line $\{x \in \mathbb{R}^2 : (x - y(\theta)) \cdot \vec{\Theta} = 0\}$ is tangent to $\mathcal{S}$.

Let $H_\epsilon(s)$, $s \in \mathbb{R}$, be a family of functions defined for all $0 < \epsilon \le \epsilon_0$, where ϵ_0 is sufficiently small, with the following properties,

$$\sup_{s\in\mathbb{R}, 0<\epsilon\le\epsilon_0} |\epsilon^{-1} H_\epsilon(s)| < \infty \text{ and } \sup_{s\in\mathbb{R}, h\neq 0, 0<\epsilon\le\epsilon_0} \frac{|H_\epsilon(s+\epsilon^{1/2}h) - H_\epsilon(s)|}{\epsilon |h|^\gamma} < \infty \tag{2.7}$$

for some γ, $0 < \gamma \le 1$. It is convenient to introduce the normalized function

$$H_0(s) := \epsilon^{-1} H_\epsilon(\epsilon^{1/2} s). \tag{2.8}$$

The dependence of H_0 on ϵ is omitted from notation for simplicity. In terms of H_0 we have $H_\epsilon(s) = \epsilon H_0(s/\epsilon^{1/2})$. Assumptions in (2.7) mean that H_0 is uniformly bounded and uniformly Hölder continuous with exponent γ. Define also

$$f_\epsilon(x) = \begin{cases} \Delta f(x), & 0 < t < H_\epsilon(\theta), \\ -\Delta f, & H_\epsilon(\theta) < t < 0, \\ 0, & \text{in all other cases}, \end{cases} \tag{2.9}$$

$$\Delta f(x) := f_+(x) - f_-(x),\ x = y(\theta) + t\vec{\Theta},\ \theta \in I.$$

As is easily seen, $f_\epsilon^{\text{mod}}(x) := f(x) - f_\epsilon(x)$ is a function, in which $\mathcal{S}$ is locally modified by H_ϵ; see Figure 1. At the points where $H_\epsilon(\theta) > 0$, a small region is removed from D_+ and added to D_- (thereby extending f_- to the region that was formerly part of D_+). At the points where $H_\epsilon(\theta) < 0$, a small region is removed from D_- and added to D_+ (thereby extending f_+ to the region that was formerly part of D_-). The magnitude of the perturbation is $O(\epsilon)$. Let $\mathcal{S}_\epsilon$ denote the perturbed boundary. Thus,

$f_\epsilon^{\mathrm{mod}}(x)$ is discontinuous across $\mathcal{S}_\epsilon$ instead of $\mathcal{S}$. Globally, the perturbed function $f_\epsilon^{\mathrm{mod}}(x)$ and the curve $\mathcal{S}_\epsilon$ are obtained by stitching together local perturbations. In this construction, the functions H_ϵ and $f_\pm$ may vary from place to place (but the latter are ϵ-independent).

In Theorem 2.5 we obtained the DTB in the case of a sufficiently smooth $\mathcal{S}$. By linearity, we can ignore the original function f and consider the reconstruction of only the perturbation f_ϵ. This follows, because the inversion formula (2.3) is linear, and the resolution of the reconstruction of f is described in Theorem 2.5.

Introduce the notation

(2.10)
$$\chi_H(t) := \begin{cases} 1, & 0 \le t \le H, \\ 0, & t \notin [0, H] \end{cases} \text{ if } H > 0, \text{ and } \chi_H(t) := \begin{cases} -1, & H \le t \le 0, \\ 0, & t \notin [H, 0] \end{cases} \text{ if } H < 0.$$

Let $f_\epsilon^{\mathrm{rec}}$ denote the reconstrution of only the perturbation f_ϵ (2.9). The first result in this paper is as follows.

THEOREM 2.6. *Let*

(a) *f satisfy Assumptions* 2.1*;*
(b) *the detector aperture function w satisfy Assumptions* 2.2*;*
(c) *the interpolation kernel φ satisfy Assumptions* 2.3*; and*
(d) *in a neighborhood of any $x_0 \in \mathcal{S}$, local perturbations H_ϵ satisfy* (2.7).

Suppose $x_0 \in \mathcal{S}$ is generic, and let θ_0 be the angle such that $\vec{\Theta}_0$ is the positive unit normal to $\mathcal{S}$ at x_0. Set $H_0 := H_\epsilon(\theta_0)/\epsilon$. If $f_\epsilon^{\mathrm{rec}}$ is the reconstruction of f_ϵ from the data (2.2) *(with $f = f_\epsilon$) using* (2.3)*, then*

$$\lim_{\epsilon \to 0} \left[f_\epsilon^{\mathrm{rec}}(x_0 + \epsilon \check{x}) - \Delta f(x_0) (\varphi * w * \chi_{H_0})(\vec{\Theta}_0 \cdot \check{x}) \right] = 0, \tag{2.11}$$

where Δf is the same as in (2.9)*. If $x_0 \notin \mathcal{S}$ is generic, then*

$$\lim_{\epsilon \to 0} f_\epsilon^{\mathrm{rec}}(x_0 + \epsilon \check{x}) = 0. \tag{2.12}$$

Even though smooth extensions of f_+ into D_- and of f_- into D_+ are not unique, this nonuniqueness is irrelevant. The statement of Theorem 2.6 does not use the values of the extensions. It involves only $\Delta f(x)$, $x \in \mathcal{S}$, which is the jump of f across $\mathcal{S}$ and is determined uniquely. This observation is similar in spirit to the remark that follows Theorem 2.5.

Comparing and combining (2.5) and (2.11) we see that a nonsmooth perturbation in $f_\epsilon^{\mathrm{mod}}(x)$ leads to the following two effects:

1. Local shifting of the reconstructed boundary $x_0 \to x_0 + H_\epsilon(\theta_0)\vec{\Theta}_0$, and
2. the DTB retains its structure of the 1 dimensional (1D) convolution of the ideal edge response (step function with the jump at $\vec{\Theta}_0 \cdot x_0 + H_\epsilon(\theta_0)$) with $\varphi * w$.

3. Beginning of the proof of Theorem 2.6. Pick a generic $x_0 \in \mathcal{S}$. By Assumptions 2.1, linearity, and the appropriate choice of coordinates we can consider only one domain $U \ni x_0$ and assume that

1. $\mathcal{S} (= \mathcal{S} \cap U)$ is sufficiently short and parametrized by $[-a, a] \ni \theta \to y(\theta)$ for some small $a > 0$;
2. $x_0 = y(0)$, so $\vec{\Theta}_0 = (1, 0)$;
3. $R(\theta) = \vec{\Theta} \cdot y''(\theta) > 0$, $|\theta| \le a$;

4. $\mathrm{supp}(f) \subset U$;
5. $f \equiv 0$ in a neighborhood of the endpoints of $\mathcal{S}$.

Recall that $\vec{\Theta}_0$ is the unit positive normal to $\mathcal{S}$ at x_0, and $R(\theta)$ is the radius of curvature of $\mathcal{S}$ at $y(\theta)$. By assumptions 1 and 5 above, $f(x) \equiv 0$ in a neighborhood of $y(\pm a)$. Using Assumption 2.1.f2 and that $\mathcal{S}$ is sufficiently short (i.e., $0 < a \ll 1$) we have

1. $y(\theta)$ is a regular parametrization with $y \in C^4([-a,a])$ (i.e., bounded derivatives up to the fourth order);
2. $\mathcal{S}$ satisfies

$$\frac{\max_{|\theta|\le a} |\vec{\Theta} \cdot y'''(\theta)|}{\min_{|\theta|\le a} R(\theta)} a \ll 1; \tag{3.1}$$

3. there exists $c > 0$ such that

$$\vec{\Theta} \cdot (x_0 - y(\theta)) \ge c\theta^2, \ |\theta| \le a; \tag{3.2}$$

4. no line $\{x \in \mathbb{R}^2 : \vec{\alpha} \cdot x = p\}$ is tangent to $\mathcal{S}$ if $a < |\alpha| \le \pi/2$.

Additional requirements on the smallness of a will be formulated later as needed.

Pick some $A \gg 1$ and define

$$\Omega_1 := \{\alpha : |\alpha| \le A\epsilon^{1/2}\}, \ \Omega_2 := [-a,a] \setminus \Omega_1, \ \Omega_3 := [-\pi/2, \pi/2] \setminus [-a,a]. \tag{3.3}$$

Let $f^{(j)}$ denote the reconstruction obtained by the formula in (2.3) with α_k restricted to Ω_j, $j = 1,2,3$. The first term is split into two: $f^{(1)} = f_1^{(1)} + f_2^{(1)}$, where $f_1^{(1)}$ is the leading singular term of $f^{(1)}$. The term $f_1^{(1)}$ is defined following (3.7) below.

The result in Theorem 2.6 involves the limit of $f_\epsilon^{\mathrm{rec}}(x_0 + \epsilon\check{x})$ as $\epsilon \to 0$. Of the three functions $f^{(j)}$ that make up $f_\epsilon^{\mathrm{rec}}$, two depend on the new parameter $A \gg 1$. The logic of our proof is based on computing the double limit $\lim_{A\to\infty} \lim_{\epsilon\to 0} f^{(j)}$, $j = 1,2$. It is important that A is fixed when the limit as $\epsilon \to 0$ is computed.

3.1. Estimation of $f_1^{(1)}$. Substitute (2.9) into (2.2):

$$\begin{aligned}
\hat{f}_\epsilon(\alpha,p) =& \frac{1}{\epsilon} \int_{-a}^{a} \int_0^{H_\epsilon(\theta)} w\left(\frac{p - \vec{\alpha}\cdot(y(\theta) + t\vec{\Theta})}{\epsilon}\right) F(\theta,t)\mathrm{d}t\mathrm{d}\theta \\
=& \int_{-a}^{a} \int_0^{\epsilon^{-1}H_\epsilon(\theta)} w\left(\hat{P} - \vec{\alpha}\cdot\frac{y(\theta)-y(\alpha)}{\epsilon} - \hat{t}\cos(\theta-\alpha)\right) F(\theta,\epsilon\hat{t})\mathrm{d}\hat{t}\mathrm{d}\theta, \\
F(\theta,t) :=& \Delta f(y(\theta) + t\vec{\Theta})(R(\theta) - t), \ \hat{P} := \frac{p - \vec{\alpha}\cdot y(\alpha)}{\epsilon}.
\end{aligned} \tag{3.4}$$

Here $R(\theta) - t = \det(\mathrm{d}y/\mathrm{d}(\theta,t))$. We assume that ϵ is sufficiently small, and $R(\theta) - t > 0$ on the domain of integration. Denote

$$\tilde{\alpha} := \alpha/\epsilon^{1/2}, \ \nu := \theta - \alpha, \ \tilde{\nu} := \nu/\epsilon^{1/2}. \tag{3.5}$$

Generally, throughout the paper a hat above a variable denotes rescaling of the original variable by a factor of ϵ, and a tilde above a variable denotes rescaling by a factor of $\epsilon^{1/2}$. For example, $\hat{p} = p/\epsilon$ and $\tilde{\alpha} = \alpha/\epsilon^{1/2}$. Then

$$\begin{aligned}
\hat{f}_\epsilon(\alpha,p) &= \epsilon^{1/2} g(\alpha, \hat{P}), \\
g(\alpha,\hat{p}) &:= \int_{\tilde{\nu}_-}^{\tilde{\nu}_+} \int_0^{\epsilon^{-1}H_\epsilon(\alpha+\epsilon^{1/2}\tilde{\nu})} w\left(\hat{p} - \vec{\alpha}\cdot\frac{y(\alpha+\epsilon^{1/2}\tilde{\nu}) - y(\alpha)}{\epsilon} - \hat{t}\cos(\epsilon^{1/2}\tilde{\nu})\right) \\
&\quad \times F(\alpha + \epsilon^{1/2}\tilde{\nu}, \epsilon\hat{t})\mathrm{d}\hat{t}\mathrm{d}\tilde{\nu}
\end{aligned}$$

$$= \int_{\tilde{\nu}_-}^{\tilde{\nu}_+} \int_0^{H_0(\tilde{\alpha}+\tilde{\nu})} w\left(\hat{p} - \left(\frac{\vec{\alpha}\cdot y''(\alpha)\tilde{\nu}^2}{2} + \frac{O(\epsilon^{3/2}|\tilde{\nu}|^3)}{\epsilon}\right) - \hat{t}\left(1+O(\epsilon\tilde{\nu}^2)\right)\right)$$

$$\times \left(\Delta f(y(\alpha))R(\alpha) + O(\epsilon^{1/2}|\tilde{\nu}|) + O(\epsilon)\right) \mathrm{d}\hat{t}\mathrm{d}\tilde{\nu}, \tag{3.6}$$

where $\tilde{\nu}_\pm = (\pm a - \alpha)/\epsilon^{1/2}$. In this subsection, $|\alpha| = O(\epsilon^{1/2})$, so $R(\alpha) - R(0) = O(\epsilon^{1/2})$, and we can replace $\vec{\alpha}\cdot y''(\alpha) = R(\alpha)$ with $R_0 = R(0)$ in the argument of w. The corresponding error term is $O(\epsilon^{1/2}\tilde{\nu}^2)$. A similar argument holds for the product $\Delta f(y(\alpha))R(\alpha)$, and the corresponding error term is $O(\epsilon^{1/2})$.

Let us look at the leading term of g, which is obtained by neglecting all the big-O terms and extending the integral with respect to $\tilde{\nu}$ to all of $\mathbb{R}$:

$$g_l(\alpha,\hat{p}) := \Delta f(x_0)R_0 \int_{\mathbb{R}} \int_0^{H_0(\tilde{\alpha}+\tilde{\nu})} w\left(\hat{p} - (R_0/2)\tilde{\nu}^2 - \hat{t}\right) \mathrm{d}\hat{t}\mathrm{d}\tilde{\nu}, \tag{3.7}$$

where $\tilde{\alpha}$ and H_0 are the same as in (3.5) and (2.8), respectively. The subscript "l" signifies that g_l is the leading term of g. By definition, substitution of the resulting approximation $\hat{f}_\epsilon(\alpha,p) \approx \epsilon^{1/2} g_l(\alpha,\hat{P})$ into (2.3) (with $\hat{P}$ as in (3.4)) and restricting the sum to $\alpha_k \in \Omega_1$ gives $f_1^{(1)}$.

LEMMA 3.1. *Fix any δ, $0<\delta<1/2$. For some c and any $\alpha\in(-a,a)$ one has*

$$g_*(\alpha,\hat{p}) \equiv 0 \text{ for } \hat{p} < c, \tag{3.8}$$

$$g_*(\alpha,\hat{p}) = O(\hat{p}^{-1/2}),\ \hat{p}\to+\infty, \tag{3.9}$$

and

$$g_*(\alpha,\hat{p}+\Delta\hat{p}) - g_*(\alpha,\hat{p}) = O\left(|\Delta\hat{p}|^\gamma \hat{p}^{-(1+\gamma)/2}\right) \text{ if } |\Delta\hat{p}| = O(\hat{p}^\delta),\ \hat{p}\to+\infty. \tag{3.10}$$

The above assertions hold for both $g_* = g$ and $g_* = g_l$. The big-O terms in (3.9) *and* (3.10) *are uniform with respect to $\alpha\in(-a,a)$ and $\epsilon>0$ sufficiently small.*

A proof of the lemma is in Appendix A. Substitute the data (2.2) into the inversion formula (2.3) and use (3.4), (3.6):

$$\frac{1}{\pi}\sum_j \int \frac{\partial_p \varphi\left(\frac{p-p_j}{\epsilon}\right)}{p-\alpha\cdot x} dp \hat{f}_\epsilon(\alpha,p_j)$$
$$= \epsilon^{-1/2}\sum_j (\mathcal{H}\varphi')\left(\frac{\alpha\cdot x-\bar{p}}{\epsilon} - j\right) g\left(\alpha, j - \frac{\alpha\cdot y-\bar{p}}{\epsilon}\right), \tag{3.11}$$

where $\mathcal{H}$ is the Hilbert transform. In this subsection we approximate $g \approx g_l$ and introduce

$$\Psi_l(\tilde{\alpha},\hat{p},q) := \sum_j (\mathcal{H}\varphi')(\hat{p}-j)\, g_l(\alpha, j-q). \tag{3.12}$$

Recall that we continue using the convention that α and $\tilde{\alpha}$ are related as in (3.5).

Even though Ψ_l depends on ϵ via g_l and H_0 (see (3.7)), this dependence is omitted from notation for simplicity. All the properties of Ψ_l to be established below are uniform with respect to ϵ and $\tilde{\alpha}$. Clearly, $\Psi_l(\tilde{\alpha},\hat{p}-n,q-n) = \Psi_l(\tilde{\alpha},\hat{p},q)$ for any $n\in\mathbb{Z}$.

We need the asymptotics of $\Psi_l(\tilde{\alpha},\hat{p},q)$ as $\hat{p}-q\to\infty$. By the invariance of Ψ_l with respect to integer shifts, we can assume that q is confined to a bounded set, e.g., $q\in[0,1)$ and $\hat{p}\to\infty$. The following result is proven in Appendix B.

LEMMA 3.2. *One has*

$$\Psi_l(\tilde{\alpha},\hat{p},q)=\begin{cases}O(|\hat{p}|^{-3/2}), & \hat{p}\to-\infty,\\ O(\hat{p}^{-(1+\delta)/2}), & \hat{p}\to+\infty,\end{cases}\quad \delta=\frac{\gamma}{\gamma+1},\ |\tilde{\alpha}|<\epsilon^{-1/2}a,\ q\in[0,1), \tag{3.13}$$

where the big-O terms are uniform with respect to $\tilde{\alpha},q$ in the indicated sets and $\epsilon>0$ sufficiently small.

From (3.4), (3.6), (3.7), (3.11), and (3.12), the leading term of the reconstruction is given by

$$\begin{aligned} f_1^{(1)}(x_0+\epsilon\check{x}) &= -\frac{1}{2\pi}\frac{\Delta\alpha}{\epsilon^{1/2}}\sum_{\alpha_k\in\Omega_1}\Psi_l\left(\frac{\alpha_k}{\epsilon^{1/2}},\frac{\vec{\alpha}_k\cdot x-\bar{p}}{\epsilon},\frac{\vec{\alpha}_k\cdot y(\alpha_k)-\bar{p}}{\epsilon}\right)\\ &= -\frac{\kappa\epsilon^{1/2}}{2\pi}\sum_{\alpha_k\in\Omega_1}\Psi_l\left(\frac{\alpha_k}{\epsilon^{1/2}},\vec{\alpha}_k\cdot\check{x}+\frac{\vec{\alpha}_k\cdot(x_0-y(\alpha_k))}{\epsilon}+q_k,q_k\right), \qquad (3.14)\\ q_k &:= \left\{\frac{\vec{\alpha}_k\cdot y(\alpha_k)-\bar{p}}{\epsilon}\right\}. \end{aligned}$$

Here $\{r\}:=r-\lfloor r\rfloor$ denotes the fractional part of r, and $\lfloor r\rfloor$ is the floor function, i.e. the largest integer not exceeding r.

LEMMA 3.3. *One has:*

$$\begin{aligned} \Psi_l(\tilde{\alpha}+\Delta\tilde{\alpha},\hat{p},q)-\Psi_l(\tilde{\alpha},\hat{p},q) &= O(|\Delta\tilde{\alpha}|^{\gamma}),\ \Delta\tilde{\alpha}\to 0,\\ \Psi_l(\tilde{\alpha},\hat{p}+\Delta\hat{p},q)-\Psi_l(\tilde{\alpha},\hat{p},q) &= O(|\Delta\hat{p}|^{\mu}),\ \Delta\hat{p}\to 0, \qquad (3.15)\\ \Psi_l(\tilde{\alpha},\hat{p},q+\Delta q)-\Psi_l(\tilde{\alpha},\hat{p},q) &= O(|\Delta q|),\ \Delta q\to 0, \end{aligned}$$

for any $\mu<1$. The big-O terms are uniform with respect to $\tilde{\alpha}\in\epsilon^{-1/2}(-a,a)$, $\hat{p}$ and q confined to any bounded set, and $\epsilon>0$ sufficiently small.

Proof. The first line follows from (2.7), (3.7), (3.12), and the fact that $\mathcal{H}\varphi'(t)=O(t^{-2})$, $t\to\infty$.

To prove the second line, note that the pseudodifferential operator $\mathcal{H}\partial/\partial t\in S^1_{1,0}(\mathbb{R}\times\mathbb{R})$ and $\varphi\in C_0^2(\mathbb{R})$, so $\mathcal{H}\varphi'\in C^1_*(\mathbb{R})$, where $C^s_*(\mathbb{R})$, $s>0$, denotes the Hölder–Zygmund space (see item 2 in Remark 6.4 and Theorem 6.19 in [1]). Since $C^1_*(\mathbb{R})\subset C^\mu_*(\mathbb{R})$ for any $\mu\in(0,1)$, and the latter space consists of functions that are Hölder continuous with exponent μ (e.g., see Theorem 6.1 in [1]), we get that

$$|\mathcal{H}\varphi'(t+\Delta t)-\mathcal{H}\varphi'(t)|\le c_1\begin{cases}|\Delta t|/(1+t^2), & |t|\ge c_2,\\ |\Delta t|^{\mu},\ |t|\le c_2\end{cases} \tag{3.16}$$

for some $c_{1,2}>0$ and all $|\Delta t|$ sufficiently small. The desired assertion now follows.

The third line follows by replacing q with $q+\Delta q$ in (3.12) and then in (3.7), subtracting $\Psi_l(\tilde{\alpha},\hat{p},q)$ from $\Psi_l(\tilde{\alpha},\hat{p},q+\Delta q)$, and then using that w is compactly supported. ∎

By (3.14) and the second line in Lemma 3.3,

$$f_1^{(1)}(x_0+\epsilon\check{x})=-\frac{\kappa\epsilon^{1/2}}{2\pi}\sum_{\alpha_k\in\Omega_1}\Psi_l\left(\frac{\alpha_k}{\epsilon^{1/2}},\vec{\Theta}_0\cdot\check{x}+\frac{R_0}{2}\frac{\alpha_k^2}{\epsilon}+q_k,q_k\right)+O(\epsilon^{\mu/2}). \tag{3.17}$$

We can use Lemma 3.3, because the arguments of Ψ_l remain bounded when $\alpha_k\in\Omega_1$. With $\tilde{\alpha}_k:=\alpha_k/\epsilon^{1/2}$, we have $\Delta\tilde{\alpha}=\kappa\epsilon^{1/2}$. Using that x_0 is generic and following the same approach as in [18] lead to (condition 2 in Definition 2.4 is essential in this step)

$$\lim_{\epsilon\to 0}\left(f_1^{(1)}(x_0+\epsilon\check{x})+\frac{1}{2\pi}\int_{|\tilde{\alpha}|\le A}\int_0^1 \Psi_l\left(\tilde{\alpha},\vec{\Theta}_0\cdot\check{x}+\frac{R_0}{2}\tilde{\alpha}^2+q,q\right)\mathrm{d}q\mathrm{d}\tilde{\alpha}\right)=0. \tag{3.18}$$

The double integral in (3.18) does not necessarily have a limit as $\epsilon\to 0$, since the dependence of H_0 and Ψ_l on ϵ (see (3.7) and (3.12)) can be complicated.

Note that the argument in this subsection establishes the limit in (3.18), but it does not say anything about the rate of convergence.

3.2. Estimation of $f_2^{(1)}$. Recall that $f_2^{(1)}$ is the less singular part of $f^{(1)}$: $f_2^{(1)}=f^{(1)}-f_1^{(1)}$, where $f_1^{(1)}$ is the leading singular term of $f^{(1)}$ and is defined following (3.7). Define (cf. (3.6) and (3.7))

$$\Delta g(\alpha,\hat{p}):=g(\alpha,\hat{p})-g_l(\alpha,\hat{p}). \tag{3.19}$$

Note that g_l (and, therefore, Δg) is not compactly supported in $\hat{p}$, even though g is compactly supported. However, inserting in (3.7) the same limits $\tilde{\nu}_\pm$ as in (3.6), introduces only a small error:

$$g_l(\alpha,\hat{p})-\Delta f(x_0)R_0\int_{\tilde{\nu}_-}^{\tilde{\nu}_+}\int_0^{H_0(\tilde{\alpha}+\tilde{\nu})} w\left(\hat{p}-(R_0/2)\tilde{\nu}^2-\hat{t}\right)\mathrm{d}\hat{t}\mathrm{d}\tilde{\nu}=O(\epsilon^{1/2}). \tag{3.20}$$

The big-O term in (3.20) is uniform with respect to α in compact subsets of $(-a,a)$. The latter condition ensures that $\tilde{\nu}_\pm=O(\epsilon^{-1/2})$. In this subsection we assume that $\alpha\in\Omega_1$, so the estimate (3.20) is indeed uniform. Since $w\in C_0^2(\mathbb{R})$ and $F\in C^2([-a,a]\times[-\delta,\delta])$ for some $\delta>0$, we have from (3.6), the paragraph following (3.6), and (3.20)

$$\begin{aligned}|\Delta g(\alpha,\hat{p})|&\le c\begin{cases}|\hat{p}|^{-1/2}\left[\epsilon^{1/2}|\hat{p}|+\epsilon^{-1}(\epsilon|\hat{p}|)^{3/2}\right], & c\le|\hat{p}|\le c/\epsilon,\\ \epsilon^{1/2}, & |\hat{p}|\le c \text{ or } |\hat{p}|\ge c/\epsilon\end{cases}\\ &\le c\epsilon^{1/2}(|\hat{p}|+1)\end{aligned} \tag{3.21}$$

for some $c>0$, which may have different values in different places. Here we have used that in (3.6), $c_1\le\tilde{\nu}^2/|\hat{p}|\le c_2$ if $|\hat{p}|\ge c_3$ for some $c_{1,2,3}>0$.

Define similarly to (3.12):

$$\Delta\Psi(\tilde{\alpha},\hat{p},q):=\sum_j(\mathcal{H}\varphi')(\hat{p}-j)\,\Delta g(\alpha,j-q). \tag{3.22}$$

Substitute (3.21) into (3.22):

$$\begin{aligned}|\Delta\Psi(\tilde{\alpha},\hat{p},q)|&\le\sum_{|j|\ge O(\epsilon^{-1})}\frac{O(\epsilon^{1/2})}{1+(\hat{p}-j)^2}+\sum_{|j|\le O(\epsilon^{-1})}\frac{O(\epsilon^{1/2})(|j|+1)}{1+(\hat{p}-j)^2}\\ &=O(\epsilon^{1/2}\ln(1/\epsilon)),\end{aligned} \tag{3.23}$$

assuming that $\hat{p}$ in (3.23) is confined to a bounded set, e.g., $|\hat{p}|\le c$. Here $c>0$ can be any fixed number. The restriction on $\hat{p}$ is justified, since $\alpha_k\in\Omega_1$. Indeed, (3.3), (3.14), and (3.17), imply that $|\hat{p}|\lesssim(R_0/2)A^2$ when $A\gg 1$. Clearly, the estimate (3.23) is uniform with respect to $\hat{p}\in[-c,c]$, $\alpha\in\Omega_1$ (i.e., $|\tilde{\alpha}|\le A$), $q\in[0,1)$, and all $\epsilon>0$ sufficiently small. Recall that $A\gg 1$ is fixed when computing the limit as $\epsilon\to 0$. Summing over all $\alpha_k\in\Omega_1$ similarly to (3.14), yields

$$f_2^{(1)}(x_0+\epsilon\check{x})=\epsilon^{1/2}\sum_{|\alpha_k|\in\Omega_1}O(\epsilon^{1/2}\ln(1/\epsilon))=O(\epsilon^{1/2}\ln(1/\epsilon)). \tag{3.24}$$

3.3. Estimation of $f^{(2)}$. Recall that $f^{(2)}$ is the reconstruction obtained by (2.3) with α_k restricted to Ω_2 (see (3.3)). From (3.6), we get, similarly to (3.14),

$$
\begin{aligned}
f^{(2)}(x_0+\epsilon\check{x}) &= -\epsilon^{1/2}\frac{\kappa}{2\pi}\sum_{\alpha_k\in\Omega_2}\Psi\left(\alpha_k,\vec{\alpha}_k\cdot\check{x}+\frac{\vec{\alpha}_k\cdot(x_0-y(\alpha_k))}{\epsilon}+q_k,q_k\right),\\
\Psi(\alpha,\hat{p},q) &:= \sum_j (\mathcal{H}\varphi')(\hat{p}-j)\,g(\alpha,j-q),
\end{aligned}
\tag{3.25}
$$

and the q_k are defined in (3.14). By Lemma 3.1, Ψ also satisfies (3.13). By (3.2),

$$
\begin{aligned}
|f^{(2)}(x_0+\epsilon\check{x})| &\le c_1\epsilon^{1/2}\sum_{\alpha_k\in\Omega_2}\left|\Psi\left(\alpha_k,\vec{\alpha}_k\cdot\check{x}+\frac{\vec{\alpha}_k\cdot(x_0-y(\alpha_k))}{\epsilon}+q_k,q_k\right)\right|\\
&\le c_2\epsilon^{1/2}\sum_{k\ge A/\epsilon^{1/2}}(k^2\epsilon)^{-(1+\delta)/2}\le c_3\int_A^\infty x^{-(1+\delta)}\mathrm{d}x = O(A^{-\delta})
\end{aligned}
\tag{3.26}
$$

for δ defined in (3.13) and some $c_{1,2,3}$. Consequently,

$$
\lim_{A\to\infty}\lim_{\epsilon\to 0} f^{(2)}(x_0+\epsilon\check{x}) = 0. \tag{3.27}
$$

3.4. Estimation of $f^{(3)}$. Following our convention, the third term $f^{(3)}$ is the reconstruction obtained by (2.3) with α_k restricted to Ω_3. By construction, $\alpha\in\Omega_3$ implies that $\alpha\cdot y'(\theta)\neq 0$, $|\theta|\le a$. Hence, we can express θ in terms of s by solving $s=\alpha\cdot y(\theta)$. Suppose, for example, that $\alpha\cdot y'(\theta)>0$. The case when this expression is negative is completely analogous. From the first line in (3.4) we find

$$
\begin{aligned}
\hat{f}_\epsilon(\alpha,\epsilon\hat{p}) &= \int_{\alpha\cdot y(-a)}^{\alpha\cdot y(a)}\int_0^{\epsilon^{-1}H_\epsilon(\theta(s))} w\left(\hat{p}-\frac{s}{\epsilon}-\hat{t}\cos(\theta(s)-\alpha)\right)F(\theta(s),\epsilon\hat{t})\mathrm{d}\hat{t}\,\theta'(s)\mathrm{d}s\\
&= \epsilon\int_{\mathbb{R}}\int_0^{\epsilon^{-1}H_\epsilon(\theta(\epsilon\hat{s}))} w\left(\hat{p}-\hat{s}-\hat{t}\cos(\theta(\epsilon\hat{s})-\alpha)\right)\mathrm{d}\hat{t}\,F_1(\epsilon\hat{s})\mathrm{d}\hat{s}+O(\epsilon^2),\\
F_1(s) &:= F(\theta(s),0)\theta'(s),
\end{aligned}
\tag{3.28}
$$

where F is defined in (3.4).

Strictly speaking, $\mathrm{d}s/\mathrm{d}\theta$ can approach zero (i.e., $\theta'(s)\to\infty$) when $\alpha\to a^+$ and $\theta\to a^-$ or $\alpha\to -a^-$ and $\theta\to -a^+$. However, $f(x)\equiv 0$ in a neighborhood of $y(\pm a)$, so $\theta'(s)$ is bounded on the support of $F(\theta(s),\epsilon\hat{t})$. Additionally, this allows us to (i) extend $F_1(s)$ from $[\alpha\cdot y(-a),\alpha\cdot y(a)]$ to $\mathbb{R}$ by zero without reducing the smoothness of F_1, and (ii) integrate with respect to $\hat{s}$ over $\mathbb{R}$.

Using (2.7) and that w is compactly supported, replace $\hat{s}$ with $\hat{p}$ in the arguments of θ and F_1 in the last integral in (3.28):

$$
\begin{aligned}
\hat{f}_\epsilon(\alpha,\epsilon\hat{p}) &= \epsilon\int\int_0^{\epsilon^{-1}H_\epsilon(\theta(\epsilon\hat{p}))} w\left(\hat{p}-\hat{s}-\hat{t}\cos(\theta(\epsilon\hat{p})-\alpha)\right)\mathrm{d}\hat{t}\,F_1(\epsilon\hat{p})\mathrm{d}\hat{s}+O(\epsilon^{1+(\gamma/2)})\\
&= \epsilon F_1(\epsilon\hat{p})H_0\left(\epsilon^{-1/2}\theta(\epsilon\hat{p})\right)+O(\epsilon^{1+(\gamma/2)}).
\end{aligned}
\tag{3.29}
$$

Substitute (3.29) into (2.3) and sum over j:

$$\begin{aligned}&\frac{1}{\epsilon}\sum_j(\mathcal{H}\varphi')\left(\frac{p-p_j}{\epsilon}\right)\left(\epsilon F_1(p_j)H_0\left(\epsilon^{-1/2}\theta(p_j)\right)+O(\epsilon^{1+(\gamma/2)})\right)\\&\qquad=I_\epsilon(\alpha,p)+O(\epsilon^{\gamma/2}),\end{aligned}\tag{3.30}$$

$$I_\epsilon(\alpha,p):=\sum_j(\mathcal{H}\varphi')\left(\frac{p-p_j}{\epsilon}\right)F_1(p_j)H_0\left(\epsilon^{-1/2}\theta(p_j)\right).$$

Since $\sum_j(\mathcal{H}\varphi')(\hat{p}-j)\equiv 0$, we have

$$I_\epsilon(\alpha,p)=\sum_j(\mathcal{H}\varphi')\left(\frac{p-p_j}{\epsilon}\right)\left(F_1(p_j)H_0\big(\epsilon^{-1/2}\theta(p_j)\big)-F_1(p)H_0\big(\epsilon^{-1/2}\theta(p)\big)\right)\tag{3.31}$$

and

$$|I_\epsilon(\alpha,p)|\le c\sum_j(1+(\hat{p}-j)^2)^{-1}\left[|\epsilon^{1/2}(j-\hat{p})|^\gamma+\frac{\epsilon|j-\hat{p}|}{1+\epsilon|j-\hat{p}|}\right]=O(\epsilon^{\gamma/2}),\tag{3.32}$$

where $\hat{p}=(p-\bar{p})/\epsilon$. The second term in brackets is written as a fraction, because F_1 is bounded. Writing it in a more conventional form $\epsilon|j-\hat{p}|$ would cause the series in the upper bound to diverge. The above estimate is uniform with respect to $\alpha\in\Omega_3$, $p\in\mathbb{R}$, and $\epsilon>0$ sufficiently small. Summing over α_k in the inversion formula we find

$$f^{(3)}(x)=c\Delta\alpha\sum_{\alpha_k\in\Omega_3}I_\epsilon(\alpha_k,\vec{\alpha}_k\cdot x)+O(\epsilon^{\gamma/2})=O(\epsilon^{\gamma/2}).\tag{3.33}$$

4. Computing the DTB. Examples. Since $A\gg 1$ can be arbitrarily large, (3.18), (3.24), (3.27), and (3.33) imply

$$\begin{aligned}&\lim_{\epsilon\to 0}\left(f_\epsilon^{\mathrm{rec}}(x_0+\epsilon\check{x})-I(\vec{\Theta}_0\cdot\check{x},\epsilon)\right)=0,\\&I(h,\epsilon):=-\frac{1}{2\pi}\int_{\mathbb{R}}\int_0^1\Psi_l\left(\tilde{\alpha},h+(R_0/2)\tilde{\alpha}^2+q,q\right)\mathrm{d}q\mathrm{d}\tilde{\alpha},\end{aligned}\tag{4.1}$$

where Ψ_l is defined in (3.12), and R_0 is the radius of curvature of $\mathcal{S}$ at $x_0=y(0)$. Recall that the dependence of $I(h,\epsilon)$ on ϵ comes from the dependence of H_0 on ϵ, and H_0 appears in the definition of Ψ_l (see (3.12)). By Lemma 3.2, the double integral above is absolutely convergent. Therefore,

$$\begin{aligned}&I(h,\epsilon):=-\frac{1}{2\pi}\lim_{\epsilon_1\to 0^+}J(h,\epsilon_1),\\&J(h,\epsilon_1):=\int_{\mathbb{R}}\int_0^1\Psi_l\left(\tilde{\alpha},h+(R_0/2)\tilde{\alpha}^2+q,q\right)e^{-\epsilon_1\tilde{\alpha}^2}\mathrm{d}q\mathrm{d}\tilde{\alpha}.\end{aligned}\tag{4.2}$$

By (3.7) and (3.12), the double integral in (4.2) transforms to the following expression:

$$\begin{aligned}J(h,\epsilon_1)=C\iint_{\mathbb{R}^2}&(\mathcal{H}\varphi')\left(h+(R_0/2)\tilde{\alpha}^2-q\right)e^{-\epsilon_1\tilde{\alpha}^2}\\&\times\int_{\mathbb{R}}\int_0^{H_0(\tilde{\alpha}+\tilde{\nu})}w\left(q-(R_0/2)\tilde{\nu}^2-\hat{t}\right)\mathrm{d}\hat{t}\mathrm{d}\tilde{\nu}\mathrm{d}q\mathrm{d}\tilde{\alpha},\ C:=\Delta f(x_0)R_0.\end{aligned}\tag{4.3}$$

We inserted an exponential factor in (4.2), since the quadruple integral in (4.3) would otherwise not be absolutely convergent. Simplifying and changing variables $u=\tilde{\alpha}+\tilde{\nu}$, $v=\tilde{\alpha}-\tilde{\nu}$, gives

$$
\begin{aligned}
J(h,\epsilon_1) &= C\iint_{\mathbb{R}^2}\int_0^{H_0(\tilde\alpha+\tilde\nu)} (\mathcal{H}\varphi' * w)\left(h+(R_0/2)(\tilde\alpha^2-\tilde\nu^2)-\hat t\right) e^{-\epsilon_1\tilde\alpha^2}\mathrm{d}\hat t\mathrm{d}\tilde\nu\mathrm{d}\tilde\alpha \\
&= \frac{C}{2}\iint_{\mathbb{R}^2} (\mathcal{H}\varphi' * w * \chi_{H_0(u)})\,(h+(R_0/2)uv)\, e^{-\epsilon_1(u+v)^2/4}\mathrm{d}u\mathrm{d}v.
\end{aligned} \tag{4.4}
$$

See (2.10) for the definition of χ_H.

Represent the integrand in terms of its Fourier transform and integrate with respect to v:

$$
\begin{aligned}
J(h,\epsilon_1) &= -\frac{C}{2}\frac{1}{2\pi}\iiint_{\mathbb{R}^3} |\lambda|\tilde\varphi(\lambda)\tilde w(\lambda)\tilde\chi_{H_0(u)}(\lambda) e^{-i\lambda(h+(R_0/2)uv)} \\
&\quad\times e^{-\epsilon_1(u+v)^2/4}\mathrm{d}u\mathrm{d}v\mathrm{d}\lambda \\
&= -\frac{C}{4\pi}\left(\frac{4\pi}{\epsilon_1}\right)^{1/2}\iint_{\mathbb{R}^2} |\lambda|\tilde\varphi(\lambda)\tilde w(\lambda)\tilde\chi_{H_0(u)}(\lambda)\exp\left(i\frac{\lambda R_0 u^2}{2}\right) \\
&\quad\times \exp\left(-\frac{(\lambda R_0)^2}{4\epsilon_1}u^2\right)\mathrm{d}u\, e^{-i\lambda h}\mathrm{d}\lambda,
\end{aligned} \tag{4.5}
$$

where tildes above functions denote the 1D Fourier transform:

$$
\tilde\varphi(\lambda) = \int \varphi(x)e^{i\lambda x}dx. \tag{4.6}
$$

The double integral in (4.5) converges absolutely, since $\tilde\varphi(\lambda) = O(\lambda^{-2})$, $\lambda\to\infty$.

Changing the variable $s = u/\epsilon_1^{1/2}$, we get by dominated convergence:

$$
\begin{aligned}
\lim_{\epsilon_1\to 0^+} J(h,\epsilon_1) &= -\frac{C}{(4\pi)^{1/2}}\iint_{\mathbb{R}^2} |\lambda|\tilde\varphi(\lambda)\tilde w(\lambda)\tilde\chi_{H_0(0)}(\lambda) \\
&\quad\times\exp\left(-\frac{(\lambda R_0)^2}{4}s^2\right)\mathrm{d}s\, e^{-i\lambda h}\mathrm{d}\lambda \\
&= -\frac{C}{R_0}\int_{\mathbb{R}} \tilde\varphi(\lambda)\tilde w(\lambda)\tilde\chi_{H_0(0)}(\lambda)\, e^{-i\lambda h}\mathrm{d}\lambda.
\end{aligned} \tag{4.7}
$$

An integrable upper bound is $c|\lambda||\tilde\varphi(\lambda)|\exp(-(\lambda R_0 s)^2/4) \in L^1(\mathbb{R}^2)$ for some $c>0$. Recall that $\tilde\varphi(\lambda)\in L^1(\mathbb{R})$ due to assumption 2.3(IK1). Finally,

$$
I(h,\epsilon) = \frac{C}{R_0}(\varphi * w * \chi_{H_0(0)})(h) = \Delta f(x_0)(\varphi * w * \chi_{H_0(0)})(h). \tag{4.8}
$$

Example 1. Constant width layer. Suppose $H_0(\theta)\equiv H$ is a constant. In this case $H_\epsilon(\theta) = \epsilon H$, and (2.5) and (2.11) are consistent with each other. Indeed, let us return to the situation in the remark following (2.9), where f_ϵ modifies the original function f. Application of (2.5) to $f_\epsilon^{\mathrm{mod}} = f - f_\epsilon$ gives (2.5), where $\vec\Theta_0\cdot\check x$ is replaced with $\vec\Theta_0\cdot\check x - H$. This is precisely what we get by subtracting (2.11) from (2.5).

Example 2. Fractal boundary. Suppose that H_ϵ is given by

$$
\begin{aligned}
&H_\epsilon(s) := \epsilon^{1-(\gamma/2)}\sum_{n=n_0(\epsilon)}^{\infty} r^{-\gamma n}\phi(r^n s), \\
&0<\gamma<1,\ r>1,\ \phi(0)=0,\ n_0(\epsilon) = c - \lfloor (1/2)\log_r\epsilon\rfloor,\ c\in\mathbb{Z},
\end{aligned} \tag{4.9}
$$

where $\phi\in C_*^\beta(\mathbb{R})$, i.e., ϕ is bounded and Hölder continuous with exponent β, $\gamma<\beta<1$. By (2.8),

$$
\begin{aligned}
H_0(s) :=& \epsilon^{-(\gamma/2)} \sum_{n=n_0(\epsilon)}^{\infty} r^{-\gamma n} \phi(r^n \epsilon^{1/2} s) \\
=& \sum_{n=c}^{\infty} r^{-\gamma(n+q_\epsilon)} \phi(r^{n+q_\epsilon} s), \ q_\epsilon = \{(1/2) \log_r \epsilon\}.
\end{aligned} \tag{4.10}
$$

The function H_0 is a real Weierstrass-type function (see [6]), which is continuous everywhere, differentiable nowhere, and its graph is a curve whose fractal dimension exceeds one [6]. See also [3] for a slightly less general case, where ϕ is $\mathbb{Z}$-periodic. It is well known that H_0 is bounded and Hölder continuous with exponent γ. From this, both properties in (2.7) follow immediately. Thus, our approach allows the analysis of reconstruction of functions with singularities along rough (e.g., fractal) curves.

5. Remote singularities. End of the proof of Theorem 2.6. In this section we pick $x_0 \notin \mathcal{S}$ and show that the reconstruction of f_ϵ from discrete data does not create artifacts in a neighborhood of x_0 (i.e., there are no nonlocal artifacts there) as long as x_0 is generic.

Without loss of generality, we may suppose that x_0 satisfies $(x_0 - y(0)) \cdot \vec{\Theta}_0 = 0$, but $x_0 \neq y(0)$. We can still use Lemma 3.2, because it deals only with tomographic data and is independent of the reconstruction point. If $x_0 \notin \mathcal{S}$, then Δf and R_0 in (3.7) are computed at the point of tangency $y(0)$. Recall that, by Lemma 3.1, Ψ satisfies Lemma 3.2 as well. Now, the function $\vec{\Theta} \cdot (x_0 - y(\theta))$ has a root of first order at $\theta = 0$ (by condition 1 in the definition of a generic point), so

$$
\begin{aligned}
&|f^{(1)}(x_0 + \epsilon \check{x}) + f^{(2)}(x_0 + \epsilon \check{x})| \\
&\leq c_1 \epsilon^{1/2} \sum_{|\alpha_k| \leq a} \left| \Psi \left(\alpha_k, \vec{\alpha}_k \cdot \check{x} + \frac{\vec{\alpha}_k \cdot (x_0 - y(\alpha_k))}{\epsilon} + q_k, q_k \right) \right| \\
&\leq c_2 \epsilon^{1/2} \sum_{k=1}^{O(\epsilon^{-1})} k^{-(1+\delta)/2} = O(\epsilon^{\delta/2}).
\end{aligned} \tag{5.1}
$$

Here δ is the same as in (3.13), Ψ is defined in (3.25), and the q_k's are defined in (3.14). In this argument we assume that $a > 0$ is sufficiently small. How small a should be depends on the distance $|x_0 - y(0)|$. This distance depends only on the properties of f, e.g., the geometry of $\mathcal{S}$, and, therefore, is fixed for any given f. So a sufficiently small $a > 0$ can be selected and then held fixed throughout the proof.

The reconstruction at $x_0 \notin \mathcal{S}$ combines contributions of two types: (1) from a neighborhood of each point of tangency (e.g., like $y(0)$), and (2) from all other segments of $\mathcal{S}$. The latter segments have the property that no line through x_0 is tangent to them. In this section we proved that contributions of the first type are $O(\epsilon^{\delta/2})$. The estimate of $f^{(3)}$ in (3.33) does not depend on the location of x_0, so it applies in the case $x_0 \notin \mathcal{S}$ as well. Using the linearity of the Radon transform and a partition of unity type of argument, (3.33) yields that the sum of all contributions of the second type is of order $O(\epsilon^{\gamma/2})$. Hence $f_\epsilon^{\text{rec}}(x_0 + \epsilon \check{x}) \to 0$ as $\epsilon \to 0$ if $x_0 \notin \mathcal{S}$, which proves (2.12). Combining with the results in section 4 (see (4.1) and (4.8)), we finish the proof of (2.11). Theorem 2.6 is proven.

6. Numerical experiments I. Our first experiment is with an oscillatory perturbation. The perturbed boundary $\mathcal{S}_\epsilon$ oscillates around a curve $\mathcal{S}$, which is the boundary of the disk centered at $x_c = (0.1, 0.2)$ with radius $R = 0.3$. The equation of

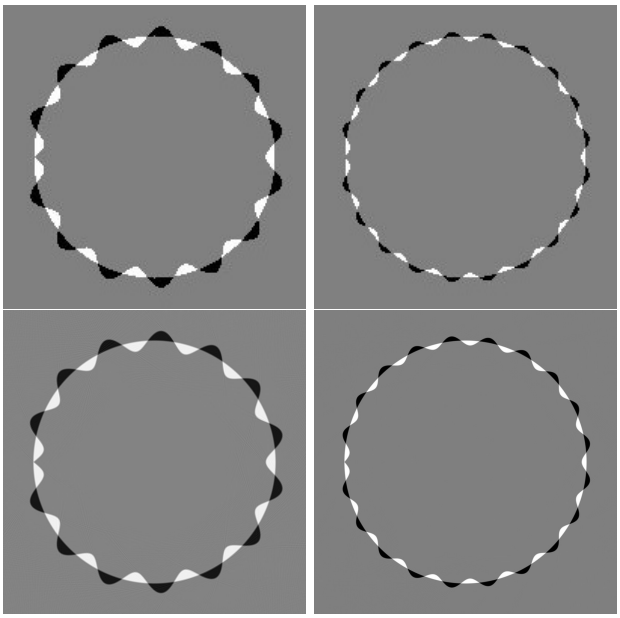

FIG. 2. *Entire oscillatory phantom, $\gamma = 1$. Left column: $N_p = 501$; right column: $N_p = 1001$. Top row: originals; bottom row: reconstructions.*

$\mathcal{S}_\epsilon$ is $r(\theta) = R + 2\epsilon\cos(0.71\theta/\epsilon^{1/2})$ in polar coordinates with the origin at the center of the disk. Here

$$\epsilon = \Delta p = 1.2/(N_p - 1),\ \Delta_\theta = \pi/N_\theta,\ N_\theta = N_p - 1.$$

Obviously, the perturbation satisfies (2.7) with $\gamma = 1$. The phantoms (i.e., the density plots of $f_\epsilon(x)$) with $N_p = 501$ and $N_p = 1001$ are shown in Figure 2.

We use the Keys interpolation kernel [23, 5]

$$\varphi(t) = 3B_3(t+2) - (B_2(t+2) + B_2(t+1)), \tag{6.1}$$

where B_n is the cardinal B-spline of degree n supported on $[0, n+1]$. The kernel is a piecewise-cubic polynomial, and φ, φ' are continuous, hence, $\varphi \in C_0^2(\mathbb{R})$.

We use this opportunity to correct the typo in [18, eq. (6.1)]. The interpolating kernel used in the numerical experiments reported in [18] was not the cubic B-spline, but the Keys kernel (6.1).

Reconstructions of a region of interest (ROI) are shown in Figures 3 and 4. The ROI is centered at the point on the boundary of the disk

$$x_0 = x_c - R(\cos(\alpha), \sin(\alpha)),\ \alpha = 0.32\pi.$$

The ROI is a square with side length 100ϵ centered at x_0. In Figure 3, $N_p = 501$, and in Figure 4, $N_p = 1001$. In this and all other figures, the gray color stands for pixel value 0, black color for pixel value (-1), and white color for pixel value 1. Notice that the ROI scales linearly with ϵ. Since the period of oscillations of $\mathcal{S}_\epsilon$ scales like $\epsilon^{1/2}$, the ROI contains fewer periods of $\mathcal{S}_\epsilon$ as ϵ decreases. Figures 3 and 4 demonstrate a good match between the DTBs (cf. Theorem 2.6) and reconstructions.

Our second experiment is with a phantom with a fractal perturbation. The fractal boundary $\mathcal{S}_\epsilon$ is around the same disk as above. The equation of $\mathcal{S}_\epsilon$ now is

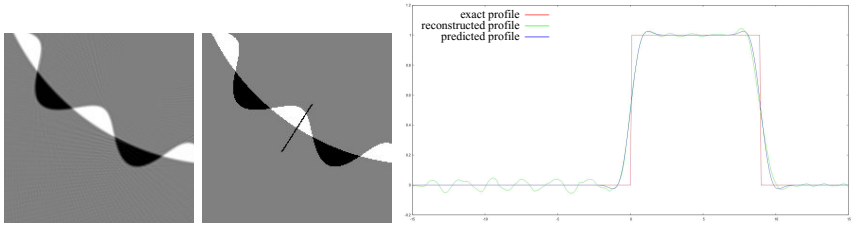

FIG. 3. *ROI in the oscillatory phantom, $\gamma = 1$, $\alpha = 0.32\pi$, $N_p = 501$. Left panel: reconstruction; middle panel: ground truth with the location of the profile shown; right panel: profiles along the line indicated in the middle panel.*

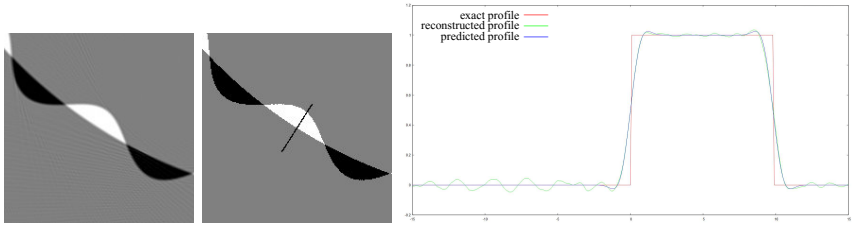

FIG. 4. *ROI in the oscillatory phantom, $\gamma = 1$, $\alpha = 0.32\pi$, $N_p = 1001$. Left panel: reconstruction; middle panel: ground truth with the location of the profile shown; right panel: profiles along the line indicated in the middle panel.*

$r(\theta) = R + \epsilon H_0(\theta/\epsilon^{1/2})$ in polar coordinates with the origin at the center of the disk, where

$$H_0(s) = 5\sum_{n=c}^{\infty} r^{-\gamma n}\sin(r^n s),\ c = \lfloor \log_r(\pi) \rfloor,\ r = \sqrt{12},\ \gamma = 1/2. \tag{6.2}$$

The phantoms with $N_p = 501$ and $N_p = 1001$ are shown in Figure 5.

Comparing Figure 3 with Figure 6 and Figure 4 with Figure 7, we see that the convergence of the reconstruction to the DTB in Theorem 2.6 is slower for smaller values of γ. The convergence is the fastest for the globally smooth boundary (close to the zero coordinate in the plots on the right in Figures 3, 4, 6, and 7), slower when $\gamma = 1$, and the slowest, when $\gamma = 0.5$.

7. New DTB. Numerical experiments II. By (2.2) and (2.3) we can write the reconstruction in the form

$$f_\epsilon^{\mathrm{rec}}(x) = -\frac{\Delta\alpha}{2\pi}\frac{1}{\epsilon^2}\sum_{|\alpha_k|\le\pi/2}\sum_j \mathcal{H}\varphi'\left(\frac{\vec{\alpha}_k\cdot x - p_j}{\epsilon}\right)\iint w\left(\frac{p_j - \vec{\alpha}_k\cdot y}{\epsilon}\right) f_\epsilon(y)\mathrm{d}y. \tag{7.1}$$

Arguing formally, the sums with respect to k and j in the limit as $\epsilon \to 0$ become integrals, and we get

$$\begin{aligned} &\lim_{\epsilon\to 0}\left(f_\epsilon^{\mathrm{rec}}(x) - \frac{1}{\epsilon^2}\iint K\left(\frac{x-y}{\epsilon}\right) f_\epsilon(y)\mathrm{d}y\right) = 0, \\ &K(z) := -\frac{1}{2\pi}\int_0^\pi (\mathcal{H}\varphi' * w)(\vec{\alpha}\cdot z)\mathrm{d}\alpha. \end{aligned} \tag{7.2}$$

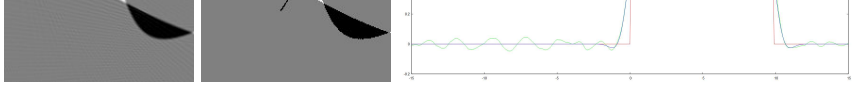

FIG. 4. *ROI in the oscillatory phantom, $\gamma = 1$, $\alpha = 0.32\pi$, $N_p = 1001$. Left panel: reconstruction, middle panel: ground truth with the location of the profile shown, right panel: profiles along the line indicated in the middle panel.*

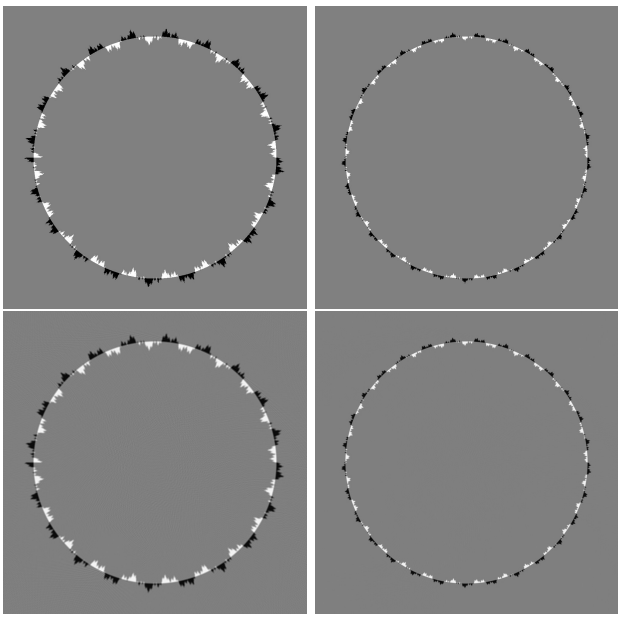

FIG. 5. *Phantom with a fractal boundary, $\gamma = 1/2$. Left column: $N_p = 501$, right column: $N_p = 1001$. Top row: ground truth, bottom row: reconstruction. Global artifacts are not visible.*

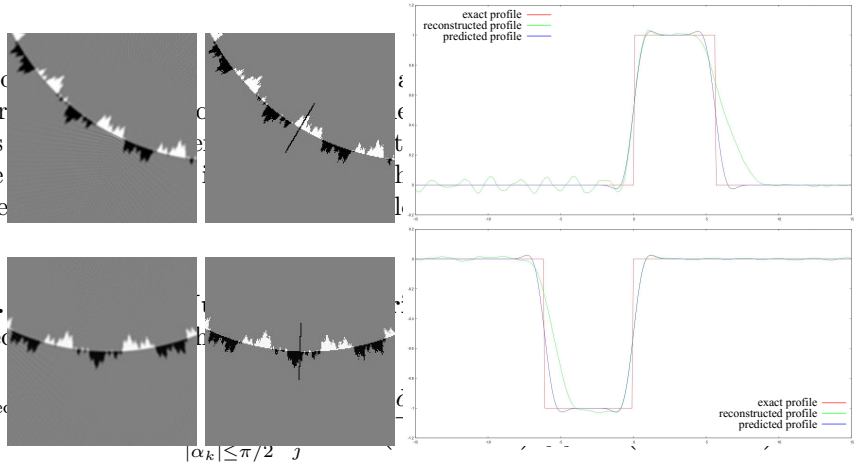

Co… …t the
conver… …naller
values … …close
to the … …, and
Figure …

7. … write
the re…
(7.1)

$$f_\epsilon^{\text{rec}} \quad \text{…} \quad y.$$

$|\alpha_k| \le \pi/2$ j

FIG. 6. *ROI in the fractal phantom, $\gamma = 1/2$, $N_p = 501$. Left column: reconstruction, middle column: ground truth with the location of the profile shown, right column: profiles along the line indicated in the middle panel. Top row: $\alpha = 0.33\pi$, bottom row: $\alpha = 0.49\pi$.*

Write (7.2) in the form of (1.3):

(7.3)
$$\text{DTB}_{\text{new}}(\check{x},\epsilon) := \frac{1}{\epsilon^2}\iint K\left(\frac{(x_0+\epsilon\check{x})-y}{\epsilon}\right) f_\epsilon(y)\mathrm{d}y,$$
$$f_\epsilon^{\text{rec}}(x_0+\epsilon\check{x}) \neq \text{DTB}_{\text{new}}(\check{x},\epsilon) + \text{error term}.$$

Obviously, K is radial and compactly supported. This follows, because $\hat{K}(\alpha,t) = (\varphi * w)(t)$ is radial, compactly supported, and even (i.e., in the range of the Radon transform). Recall that $\hat{K}$ denotes the Radon transform of K.

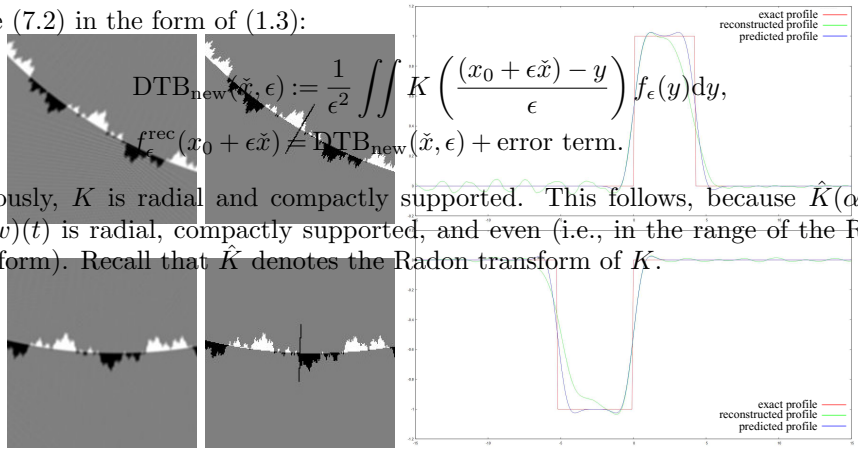

FIG. 7. *ROI in the fractal phantom, $\gamma = 1/2$, $N_p = 1001$. Left column: reconstruction, middle column: ground truth with the location of the profile shown, right column: profiles along the line*

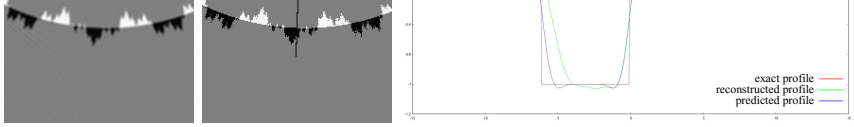

FIG. 6. *ROI in the fractal phantom, $\gamma = 1/2$, $N_p = 501$. Left column: reconstruction, middle column: ground truth with the location of the profile shown, right column: profiles along the line indicated in the middle panel. Top row: $\alpha = 0.38\pi$, bottom row: $\alpha = 0.49\pi$.*

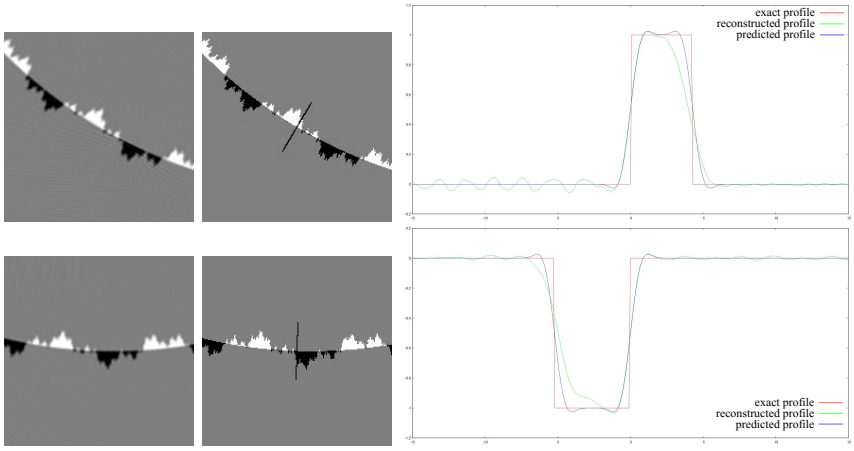

FIG. 7. *ROI in the fractal phantom, $\gamma = 1/2$, $N_p = 1001$. Left column: reconstruction, middle column: ground truth with the location of the profile shown, right column: profiles along the line indicated in the middle panel. Top row: $\alpha = 0.38\pi$, bottom row: $\alpha = 0.49\pi$.*

We see that (7.3) is easy to implement and easy to analyze in order to investigate the resolution of reconstruction from discrete data. Also, (7.2), if it is correct, implies the result proven earlier. Intuitively, as $\epsilon \to 0$, the boundaries $\mathcal{S}$ and $\mathcal{S}_\epsilon$ become locally flat, and we get Theorem 2.6. To see this fact rigorously, start similarly to (3.4),

$$f_\epsilon^{\text{rec}}(x) = \frac{1}{\epsilon^2}\iint K\left(\frac{x-y}{\epsilon}\right) f_\epsilon(y)\,\mathrm{d}y, \tag{7.2}$$

$$K(z) := -\frac{1}{2\pi}\int_0^\pi (\mathcal{H}\varphi' * w)(\vec{\alpha}\cdot z)\mathrm{d}\alpha. \tag{7.4}$$

Write (7.2) in the form of (1.3):

$$\text{DTB}_{\text{new}}(\check{x},\epsilon) := \frac{1}{\epsilon^2}\int_{-a/\epsilon}^{a/\epsilon}\int_0^{\epsilon^{-1}H_\epsilon(\epsilon\hat{\theta})} K\left(\frac{(x_0+\epsilon\check{x})-(y(\epsilon\hat{\theta})+\epsilon\hat{t}\vec{\Theta})}{\epsilon}\right) F(\epsilon\hat{\theta},\epsilon\hat{t})\mathrm{d}\hat{t}\mathrm{d}\hat{\theta}, \tag{7.3}$$

$$f_\epsilon^{\text{rec}}(x_0+\epsilon\check{x}) = \text{DTB}_{\text{new}}(\check{x},\epsilon) + \text{error term},$$

where F is the same as in (3.4). Since K is compactly supported, it is clear that $\hat{\theta}$ is confined to a bounded set, and

$$\text{DTB}_{\text{new}}(\check{x},\epsilon) = F(0,0)\int_{\mathbb{R}}\int_0^{H_0(\epsilon^{1/2}\hat{\theta})} K\left(\check{x}-\left(\hat{\theta}y'(0)+\hat{t}\vec{\Theta}_0\right)\right)\mathrm{d}\hat{t}\mathrm{d}\hat{\theta}+O(\epsilon), \tag{7.5}$$

where $H_0(\epsilon^{1/2}\hat{\theta}) = H_0(0)+O(\epsilon^{\gamma/2})$, and we used that $x_0 = y(0)$. Using that $F(0,0) = \Delta f(x_0)R_0$ and $|y'(0)| = R_0$, we compute

$$\text{DTB}_{\text{new}}(\check{x},\epsilon) = \Delta f(x_0)\int_{\mathbb{R}}\int_0^{H_0(0)} \hat{K}\left(\vec{\Theta}_0,\vec{\Theta}_0\cdot\check{x}-\hat{t}\right)\mathrm{d}\hat{t}\mathrm{d}\hat{\theta}+O(\epsilon^{\gamma/2}). \tag{7.6}$$

Recalling that $\hat{K} = \varphi * w$, the assertion follows.

Moreover, the local convergence of $\mathcal{S}_\epsilon$ to a flat line segment (which is described in terms of the convergence $H_0(\epsilon^{1/2}\hat{\theta}) \to H_0(0)$) is slower the lower the value of γ is, which matches the observations in section 6. Thus, (7.3) has the potential to be a more accurate result than that given in Theorem 2.6. Our numerical experiments confirm this conjecture. We implemented the kernel $K(z)$ and convolved it with f_ϵ to compute DTB_{new} for the same two values of ϵ. The graphs along the same line segments as in

in terms of the convergence $H_0(\epsilon^{1/2}\theta) \to H_0(0)$) is slower the lower the value of γ is, which matches the observations in section 6. Thus, (7.3) has the potential to be a more accurate result than that given in Theorem 2.6. Our numerical experiments confirm this conjecture. We implemented the kernel $K(z)$ and convolved it with f_ϵ to compute DTB_{new} for the same two values of ϵ. The graphs along the same line segments as in Figure 6 and Figure 7 are shown in Figure 8 and Figure 9, respectively. By comparing the profiles we see that the latter are significantly more accurate than the former.

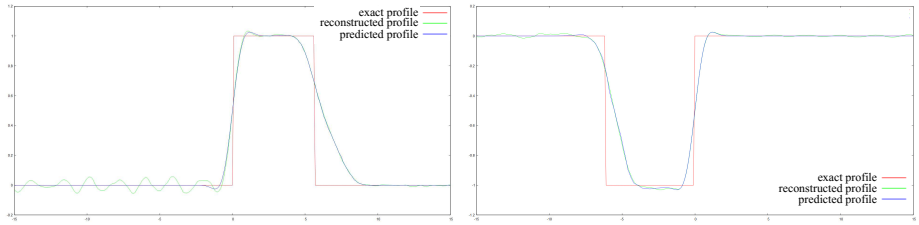

FIG. 8. *ROI in the fractal phantom of Figure 6, $\gamma = 1/2$, $N_p = 501$. Left: $\alpha = 0.33\pi$, right: $\alpha = 0.49\pi$.*

FIG. 8. *ROI in the fractal phantom of Figure 6, $\gamma = 1/2$, $N_p = 501$. Left: $\alpha = 0.33\pi$, right: $\alpha = 0.49\pi$.*

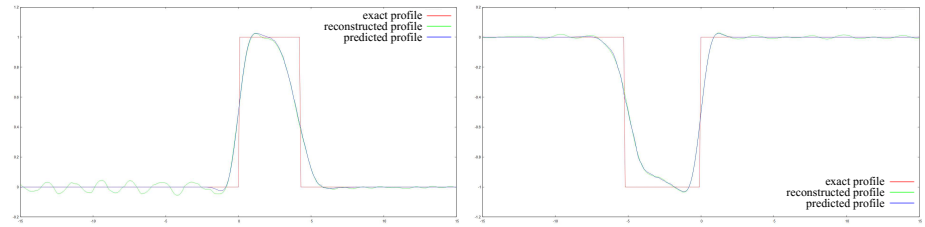

FIG. 9. *ROI in the fractal phantom of Figure 7, $\gamma = 1/2$, $N_p = 1001$. Left: $\alpha = 0.33\pi$, right: $\alpha = 0.49\pi$.*

FIG. 9. *ROI in the fractal phantom of Figure 7, $\gamma = 1/2$, $N_p = 1001$. Left: $\alpha = 0.33\pi$, right: $\alpha = 0.49\pi$.*

Figures 6 and 7 are shown in Figures 8 and 9, respectively. By comparing the profiles we see that the latter are significantly more accurate than the former.

Due to the division by ϵ, the sums with respect to j and k in (7.1) involve stepsizes that do not go to zero as $\epsilon \to 0$. Therefore, replacing the sums with integrals in (7.1) appears counterintuitive. In general, (7.2) is indeed false. This can be seen, for example, as follows. Since the kernel K is compactly supported, formula (7.2) does not explain non-local artifacts, which are known to arise in case f has a singularity across a line segment. Thus, at best, (7.2) holds only for certain classes of functions. Our numerical experiments suggest that the formula holds for functions described in section 2. The complete proof of (7.2) is complicated and beyond the scope of this paper. In this section we state one result along these lines and formulate a conjecture about the rate of convergence in (7.2). A complete explanation of our numerical results requires establishing the convergence rates in (2.11) and (7.2), and making sure that the latter is faster than the former.

Here we strengthen assumption 2.3(IK1) by requesting that $\tilde{\varphi}(\lambda) = O(|\lambda|^{-3})$, $\lambda \to \infty$. The Keys interpolation kernel in (6.1) satisfies this assumption. Consider the function

$$\psi(q,t) := \sum_j (\mathcal{H}\varphi')(q-j)w(j-q-t). \tag{7.7}$$

Then

$$\psi(q,t) = \psi(q+1,t),\ q,t \in \mathbb{R}; \quad \psi(q,t) = O(t^{-2}),\ t \to \infty,\ q \in \mathbb{R}, \tag{7.8}$$

$$\int \psi(q,t)\mathrm{d}t \equiv 0,\ q \in \mathbb{R}.$$

The last property follows from assumption 2.3(IK2), see (2.4). By (7.8), we can represent $\psi(q,t)$ in terms of its Fourier series:

$$\psi(q,t) = \sum_m \tilde{\psi}_m(t)e(-mq),\ e(q) := \exp(2\pi i q), \tag{7.9}$$

in terms of

$$\tilde{\psi}_m(t) = \int_0^1 \psi(q,t)e(mq)\mathrm{d}q = \int_{\mathbb{R}} (\mathcal{H}\varphi')(q)w(-q-t)e(mq)\mathrm{d}q.$$

Due to the assumptions that $\varphi, w \in C_0^2(\mathbb{R})$ and $\tilde{\varphi}(\lambda) = O(|\lambda|^{-3})$ we have

$$|\tilde{\psi}_m(t)| \le c(1+m^2)^{-1}(1+t^2)^{-1}, \tag{7.10}$$

for some c, so the Fourier series for ψ converges absolutely. Indeed, if t is restricted to any compact set, the result follows because $(\mathcal{H}\varphi')(\lambda), \tilde{w}(\lambda) = O(\lambda^{-2})$ implies

$$\begin{aligned}&\psi(q,t)=\sum_m \tilde{\psi}_m(t)e(-mq),\ \ e(q):=\exp(2\pi iq),\\ &\tilde{\psi}_m(t)=\int_0^1 \psi(q,t)e(mq)\mathrm{d}q=\int_{\mathbb{R}}(\mathcal{H}\varphi')(q)w(-q-t)e(mq)\mathrm{d}q.\end{aligned}\tag{7.9}$$

Due to the assumptions that $\varphi, w\in C_0^2(\mathbb{R})$ and $\tilde{\varphi}(\lambda)=O(|\lambda|^{-3})$ we have

$$|\tilde{\psi}_m(t)|\le c(1+m^2)^{-1}(1+t^2)^{-1}\tag{7.10}$$

for some c, so the Fourier series for ψ converges absolutely. Indeed, if t is restricted to any compact set, the result follows because $\widetilde{(\mathcal{H}\varphi')}(\lambda), \tilde{w}(\lambda)=O(\lambda^{-2})$ implies

$$\left|\int |\mu|\tilde{\varphi}(\mu)\tilde{w}(\mu-\lambda)e^{i(\mu-\lambda)t}\mathrm{d}\mu\right|\le\int|\mu\tilde{\varphi}(\mu)\tilde{w}(\mu-\lambda)|\mathrm{d}\mu=O(\lambda^{-2}),\lambda=2\pi m\to\infty.\tag{7.11}$$

If $|t|\ge c$ for some $c\gg 1$ sufficiently large, integrate by parts twice and use that

$$\max_q|(\partial/\partial q)^2((\mathcal{H}\varphi')(q)w(-q-t))|=O(t^{-2}),\ t\to\infty.\tag{7.12}$$

Differentiation by parts works, because $(\mathcal{H}\varphi')(q)$ is smooth in a neighborhood of any q such that $w(-q-t)\neq 0$.

From (7.1), (7.7), and (7.9), the reconstructed image becomes

$$\begin{aligned}&f_\epsilon^{\mathrm{rec}}(x)=-\frac{\Delta\alpha}{2\pi}\sum_m\sum_k e\left(-mq_k\right)A_m(\alpha_k,\epsilon),\ \sum_k:=\sum_{|\alpha_k|\le\pi/2},\\ &q_k:=\frac{\vec{\alpha}_k\cdot x-\bar{p}}{\epsilon},\ A_m(\alpha,\epsilon):=\epsilon^{-2}\iint\tilde{\psi}_m\left(\frac{\vec{\alpha}\cdot(y-x)}{\epsilon}\right)f_\epsilon(y)\mathrm{d}y.\end{aligned}\tag{7.13}$$

Suppose first that $x_0=y(0)$. To obtain (7.2), we should be able to replace the sum with respect to k by an integral with respect to α and ignore all $m\neq 0$ terms. The results in sections 3 and 5 suggest that the rate in (2.11) is $O(\epsilon^{\gamma/2})$; cf. (3.33). Thus, to establish that the new DTB is more accurate, we need to show that

$$\begin{aligned}&\Delta\alpha\sum_{m\neq0}\sum_k e\left(-mq_k\right)A_m(\alpha_k,\epsilon)=o(\epsilon^{\gamma/2}),\\ &\frac{1}{2\pi\epsilon^2}\sum_k\iint\int_{\alpha_k-\Delta\alpha/2}^{\alpha_k+\Delta\alpha/2}\left(\tilde{\psi}_0\left(\frac{\vec{\alpha}\cdot(y-x)}{\epsilon}\right)-\tilde{\psi}_0\left(\frac{\vec{\alpha}_k\cdot(y-x)}{\epsilon}\right)\right)\mathrm{d}\alpha\\ &\qquad\times f_\epsilon(y)\mathrm{d}y=o(\epsilon^{\gamma/2}).\end{aligned}\tag{7.14}$$

Suppose now $x_0\neq y(0)$, which is equivalent to assuming $x_0\notin\mathcal{S}$. In this case f is smooth near x_0, so we should expect that $\mathrm{DTB}(\check{x},\epsilon)\equiv 0$ for all $\epsilon>0$ sufficiently small. Since $K(z)$ is compactly supported, $\iint K((x-y)/\epsilon)f_\epsilon(y)\mathrm{d}y\equiv 0$ for all $\epsilon>0$ sufficiently small and all x sufficiently close to x_0, precisely as expected. Hence, there is no need to single out the term $m=0$ (which previously gave the only nonzero contribution) in (7.13), because the entire sum should go to zero sufficiently fast as $\epsilon\to 0$. The following lemma states that this is indeed the case. Its proof is in Appendix C.

LEMMA 7.1. *Pick $x_0 \notin \mathcal{S}$ such that no line through x_0, which intersects $\mathcal{S}$, is tangent to $\mathcal{S}$. This includes the endpoints of $\mathcal{S}$, in which case the one-sided tangents to $\mathcal{S}$ are considered. Suppose the level sets of H_0 are not too dense, i.e., there exist $\rho, L_0 > 0$ independent of $\hat{t}$ and ϵ such that any open interval of any length $L \geq L_0$ contains no more than ρL points from $H_0^{-1}(\hat{t})$ for almost all $\hat{t}$ and all $0 < \epsilon \leq \epsilon_0$. Under the assumptions of Theorem* 2.6*, one has*

$$f_\epsilon^{\mathrm{rec}}(x) = O(\epsilon^{1/2} \ln(1/\epsilon)),\ \epsilon \to 0, \tag{7.15}$$

uniformly with respect to x in a sufficiently small neighborhood of x_0.

Using numerical evidence and the above lemma as a guide, we state the following conjecture.

CONJECTURE 7.2. *Pick any generic x_0. Suppose the level sets of H_0 are not too dense, as defined in Lemma* 7.1*. Under the assumptions of Theorem* 2.6*, one has*

$$f_\epsilon^{\mathrm{rec}}(x_0 + \epsilon\check{x}) = \frac{1}{\epsilon^2} \iint K\left(\frac{(x_0 + \epsilon\check{x}) - y}{\epsilon}\right) f_\epsilon(y)\mathrm{d}y + O(\epsilon^{1/2} \ln(1/\epsilon)),\ \epsilon \to 0, \tag{7.16}$$

where the big-O term is uniform with respect to $\check{x}$ in any compact set.

To prove the conjecture one has to consider the case $x_0 \in \mathcal{S}$ as well as the case $x_0 \notin \mathcal{S}$, when a line through x_0 is tangent to $\mathcal{S}$.

The assumptions in Lemma 7.1 and the conjecture are not vacuous in the following sense. If H_0 is Hölder continuous, and its level sets $H_0^{-1}(\hat{t})$ are not too dense, as defined in Lemma 7.1, this does not imply that H_0 is Lipschitz continuous. In (D.1) we present an example of a function on $[0, \infty)$ (the Schwarz function [42]), which is strictly monotonically increasing, locally Hölder continuous with exponent $\gamma \in (0, 1)$, and is not locally Hölder continuous with any exponent $\gamma' > \gamma$ on any interval. Using this function as a building block, one can create a wide range of perturbations H_0, which satisfy all the assumptions in Lemma 7.1. Due to the limited smoothness of such an H_0, the derivation in section 3, section 5 for the original DTB cannot guarantee convergence faster than $O(\epsilon^{\gamma/2})$, which is slower than the conjectured rate.

Another interesting class of perturbations with limited smoothness, to which Lemma 7.1 applies, can be constructed using the Cantor staircase $c(x) : [0, 1] \to [0, 1]$ [24]. Let $C \subset [0, 1]$ be the Cantor set. Then c is increasing, the range of c is $[0, 1]$, $c([0, 1] \setminus C)$ consists of dyadic reals (i.e., numbers of the form $j2^{-m}$, $j \in \mathbb{Z}$, $m \in \mathbb{N}$), and C cannot contain any interval of nonzero length. Hence, for almost all $\hat{t} \in [0, 1]$ (i.e., for $\hat{t}$ not a dyadic real), the level set $c^{-1}(\hat{t})$ consists of a single number. The Cantor function is Hölder continuous with exponent $\gamma = \log 2/\log 3$, and no higher exponent works [8, Proposition 10.1].

Our numerical experiments show that even when the level sets of a function become infinitely dense (see [39, 43] regarding level sets of the Weirstrass function), $\mathrm{DTB}_{\mathrm{new}}$ still appears to exhibit rapid convergence faster than $O(\epsilon^{\gamma/2})$.

Appendix A. Proof of Lemma 3.1. We prove the lemma in the more complicated case $g_* = g$. The case $g_* = g_l$ is proven along the same lines, but many of the steps are simpler. Throughout this section, by c we denote various positive constants whose value in different places is different. Pick any $\alpha \in (-a, a)$. Introduce

$$\psi(\nu) := \vec{\alpha} \cdot (y(\alpha + \nu) - y(\alpha)),\ |\alpha|, |\alpha + \nu| \leq a. \tag{A.1}$$

The dependence of ψ on α is irrelevant and omitted from notation. Since $\psi^{(k)}(\nu) = \vec{\alpha} \cdot y^{(k)}(\alpha+\nu)$, $k=1,2$, we easily get from (3.1) the following properties:

$$\psi(0) = \psi'(0) = 0,\ \psi'(\nu)/\nu \geq c,\ \text{and}\ \psi''(\nu) \geq c \text{ if } |\alpha|, |\alpha+\nu| \leq a. \tag{A.2}$$

Therefore, by (3.6)

$$g(\alpha, \hat{p}) \equiv 0 \text{ for } \hat{p} < -c \tag{A.3}$$

for some c independent of $\alpha \in (-a, a)$.

Suppose now $\hat{p} \to +\infty$. Since w is compactly supported and H_0 is bounded, we can find $c > 0$ sufficiently large and independent of $\hat{p}$, ϵ, so that the domain of integration with respect to ν in (3.6) is contained inside the union of two nonintersecting intervals, whose endpoints are computed by solving

$$\psi(\epsilon^{1/2}\tilde{\nu}) = \epsilon(\hat{p} \pm c). \tag{A.4}$$

The positive pair of solutions $\tilde{\nu}_{1,2}^{+} > 0$ determines one interval, the negative pair $\tilde{\nu}_{1,2}^{-} < 0$, the other, and the two intervals are bounded away from zero. By (A.2), we get that

$$\left| \mathrm{d}\left[\epsilon^{-1}\psi(\epsilon^{1/2}\tilde{\nu})\right]/\mathrm{d}\tilde{\nu} \right| \geq c,\ \tilde{\nu} \in [\tilde{\nu}_1^{\pm}, \tilde{\nu}_2^{\pm}]. \tag{A.5}$$

Hence, again by (A.2), $\tilde{\nu}_2^{\pm} - \tilde{\nu}_1^{\pm} = O(\epsilon^{1/2}/|\psi'(\epsilon^{1/2}\tilde{\nu}_1^{\pm})|) = O(\hat{p}^{-1/2})$. The statement (3.9) follows because the integrand in (3.6) is uniformly bounded.

To prove the last assertion of the lemma, set $g = g^{+} + g^{-}$, where

$$\begin{aligned} g^{+}(\alpha, \hat{p}) = \int_0^{\epsilon^{-1/2}(a-\alpha)} \int_0^{H_0(\tilde{\alpha}+\tilde{\nu})} & w\left(\hat{p} - \psi(\epsilon^{1/2}\tilde{\nu}) - \hat{t}\cos(\epsilon^{1/2}\tilde{\nu})\right) \\ & \times F(\alpha + \epsilon^{1/2}\tilde{\nu}, \epsilon\hat{t})\mathrm{d}\hat{t}\mathrm{d}\tilde{\nu}, \end{aligned} \tag{A.6}$$

$\tilde{\alpha} = \epsilon^{-1/2}\alpha$, and g^{-} is defined similarly by integrating over $(\epsilon^{-1/2}(-a-\alpha), 0]$ with respect to $\tilde{\nu}$. First, we consider g^{+}, so $\tilde{\nu} > 0$. Introduce the variable $\hat{s} = \psi(\epsilon^{1/2}\tilde{\nu})/\epsilon$. By (A.5), $\tilde{\nu}'(\hat{s})$ is uniformly bounded for all $\epsilon > 0$ small enough whenever $\hat{s}$ is bounded away from zero. To indicate the dependence of $\tilde{\nu}(\hat{s})$ on ϵ we write $\tilde{\nu}_\epsilon(\hat{s})$. Change variables $\tilde{\nu} = \tilde{\nu}_\epsilon(\hat{s})$ in (A.6):

$$\begin{aligned} g^{+}(\alpha, \hat{p}) = \int_{\mathbb{R}} \int_0^{H_0(\tilde{\alpha}+\tilde{\nu})} & w\left(\hat{p} - \hat{s} - \hat{t}\cos(\epsilon^{1/2}\tilde{\nu})\right) F(\alpha + \epsilon^{1/2}\tilde{\nu}, \epsilon\hat{t})\mathrm{d}\hat{t}\,\tilde{\nu}_\epsilon'(\hat{s})\mathrm{d}\hat{s}, \\ & \tilde{\nu} = \tilde{\nu}_\epsilon(\hat{s}). \end{aligned} \tag{A.7}$$

Here we extended the integration with respect to $\hat{s}$ to $\mathbb{R}$. Even though $\tilde{\nu}_\epsilon'(\hat{s})$ is not defined for $\hat{s} > 0$ sufficiently large, this is irrelevant because $F(\cdot) \equiv 0$ for such $\hat{s}$. Using the argument following (3.28), such an extension does not affect the smoothness of F. Changing the lower limit does not change the integral either, because w is compactly suported and $\hat{p} \to +\infty$. Similarly,

$$\begin{aligned} g^{+}(\alpha, \hat{p} + \Delta\hat{p}) = \int_{\mathbb{R}} \int_0^{H_0(\tilde{\alpha}+\tilde{\nu})} & w\left(\hat{p} - \hat{s} - \hat{t}\cos(\epsilon^{1/2}\tilde{\nu})\right) \\ & \times F(\alpha + \epsilon^{1/2}\tilde{\nu}, \epsilon\hat{t})\mathrm{d}\hat{t}\,\tilde{\nu}_\epsilon'(\hat{s} + \Delta\hat{p})\mathrm{d}\hat{s},\ \tilde{\nu} = \tilde{\nu}_\epsilon(\hat{s} + \Delta\hat{p}). \end{aligned} \tag{A.8}$$

As before, from (A.2) we obtain

$$\tilde{\nu}_\epsilon^{(k)}(\hat{p}) = O\left(\hat{p}^{1/2-k}\right),\ \hat{p}\to+\infty,\ k=0,1,2, \tag{A.9}$$

uniformly in ϵ.

By (A.9), dropping $\Delta\hat{p}$ in the argument of $\tilde{\nu}_\epsilon$ in the argument of H_0 in the upper limit of the inner integral in (A.8) leads to an error of magnitude

$$\hat{p}^{-1/2} O\left((|\Delta\hat{p}|/\hat{p}^{1/2})^\gamma\right). \tag{A.10}$$

Recall that $\Delta\hat{p} = O(\hat{p}^\delta)$, $\delta < 1/2$, $\hat{p}\to+\infty$. Dropping $\Delta\hat{p}$ in $\tilde{\nu}_\epsilon$, which is located in the arguments of w and F, leads to an error of magnitude $(\epsilon/\hat{p})^{1/2} O(|\Delta\hat{p}|/\hat{p}^{1/2})$. Dropping $\Delta\hat{p}$ from $\tilde{\nu}_\epsilon'$ leads to an error of magnitude $O(|\Delta\hat{p}|/\hat{p}^{3/2})$.

Under our assumptions $\gamma<1$ and $\delta<1/2$, so all the error terms are dominated by (A.10). Subtracting (A.7) from (A.8) we prove that $g^+(\alpha,\hat{p})$ satisfies the estimate in (3.10). Similar arguments and similar estimates hold for $g^-(\alpha,\hat{p})$ as well, and (3.10) is proven.

Appendix B. Proof of Lemma 3.2. Using that $(\mathcal{H}\varphi')(t) = O(t^{-2})$, $t\to\infty$, we obtain for some c using (3.8), (3.9),

$$|\Psi_l(\tilde{\alpha},\hat{p},q)| \le c\sum_{j\ge -c} \frac{1}{1+(|\hat{p}|+j)^2}\frac{1}{1+|j|^{1/2}} = O(|\hat{p}|^{-3/2}),\ \hat{p}\to-\infty,\ q\in[0,1). \tag{B.1}$$

Fix any δ, $0<\delta<1/2$. Similarly to (B.1), we can show that

$$\sum_{|j-\hat{p}|\ge \hat{p}^\delta} (\mathcal{H}\varphi')(\hat{p}-j)\, g_l(\alpha, j-q) = O(\hat{p}^{-(1/2+\delta)}),\ \hat{p}\to+\infty,\ q\in[0,1). \tag{B.2}$$

Split the remaining sum into two:

$$\begin{aligned}
&\sum_{|j-\hat{p}|<\hat{p}^\delta} (\mathcal{H}\varphi')(\hat{p}-j)\, g_l(\alpha, j-q)\\
&\quad= \sum_{|j-\hat{p}|<\hat{p}^\delta} (\mathcal{H}\varphi')(\hat{p}-j)\,(g_l(\alpha,j-q)-g_l(\alpha,\hat{p}-q))\\
&\qquad+ g_l(\alpha,\hat{p}-q)\sum_{|j-\hat{p}|<\hat{p}^\delta}(\mathcal{H}\varphi')(\hat{p}-j) =: S_1+S_2.
\end{aligned} \tag{B.3}$$

Clearly, $\mathcal{H}\varphi'(t) = O(t^{-2})$, $t\to\infty$. Combining with (2.7), (3.9), and (3.10), we find

$$S_1 = O\left(\hat{p}^{\gamma(\delta-1/2)-1/2}\right)\sum_{|j-\hat{p}|<\hat{p}^\delta}(\mathcal{H}\varphi')(\hat{p}-j) = O\left(\hat{p}^{\gamma(\delta-1/2)-1/2}\right),\ \hat{p}\to+\infty. \tag{B.4}$$

Moreover, by the exactness of φ (assumption 2.3.IK2),

$$\sum_{|j-\hat{p}|<\hat{p}^\delta}\varphi'(r-j)\ne 0 \text{ only if } |r-(\hat{p}-\hat{p}^\delta)|\le c \text{ or } |r-(\hat{p}+\hat{p}^\delta)|\le c \tag{B.5}$$

for some c. Hence,

$$S_2 = O\left(\hat{p}^{-1/2}(1+\hat{p}^{2\delta})^{-1}\right) = O\left(\hat{p}^{-1/2-2\delta}\right),\ \hat{p}\to+\infty,\ q\in[0,1). \tag{B.6}$$

Combining (B.2), (B.3), (B.4), and (B.6) gives

$$|\Psi_l(\tilde{\alpha},\hat{p},q)| = O(\hat{p}^{-(1/2+\delta)}),\ \delta=(\gamma/2)/(\gamma+1),\ \hat{p}\to+\infty,\ q\in[0,1). \tag{B.7}$$

The choice of δ in (B.7) satisfies $0<\delta<1/2$ and provides the fastest guaranteed rate of decay of Ψ_l. Combining (B.1) and (B.7) (and replacing δ with $\delta/2$ for notational convenience) proves the lemma.

Appendix C. Proof of Lemma 7.1. Pick any x sufficiently close to x_0. All the estimates below are uniform with respect to x in a small (but fixed) size neighborhood, so the x-dependence of various quantities is omitted from the notation.

Let Ω be the set of all $\alpha \in [-\pi/2, \pi/2]$ such that the lines $\{y \in \mathbb{R}^2 : (y-x)\cdot\vec{\alpha} = 0\}$ intersect $\mathcal{S}$. Let $\theta = \Theta(\alpha)$, $\alpha \in \Omega$, be determined by solving $(y(\theta)-x)\cdot\vec{\alpha} = 0$. By using a partition of unity, if necessary, we can assume that $\mathcal{S}$ is short and the solution is unique. By assumption, the intersection is transverse for any $\alpha \in \Omega$ (up to the endpoints). Hence $|\Theta'(\alpha)| = |y(\Theta(\alpha)) - x|/|\vec{\alpha}\cdot y'(\Theta(\alpha))|$ and

$$0 < \min_{\alpha\in\Omega} |\vec{\alpha}\cdot y'(\Theta(\alpha))|,\ 0 < \min_{\alpha\in\Omega} |\Theta'(\alpha)| \le \max_{\alpha\in\Omega} |\Theta'(\alpha)| < \infty. \tag{C.1}$$

Transform the expression for A_m (cf. (7.13)) similarly to (3.4),

$$A_m(\alpha,\epsilon) = \frac{1}{\epsilon}\int_{-a}^{a}\int_0^{\epsilon^{-1}H_\epsilon(\theta)} \tilde{\psi}_m\left(\frac{\vec{\alpha}\cdot(y(\theta)-x)}{\epsilon} + \hat{t}\cos(\theta-\alpha)\right) F(\theta,\epsilon\hat{t})\mathrm{d}\hat{t}\mathrm{d}\theta, \tag{C.2}$$

where F is the same as in (3.4), and $\tilde{\psi}_m$ is introduced in (7.9). Clearly,

$$A_m(\alpha,\epsilon) = (1+m^2)^{-1}O(\epsilon),\ \alpha \in [-\pi/2,\pi/2]\setminus\Omega. \tag{C.3}$$

Next, consider the case $\alpha \in \Omega$. Setting $\tilde{\theta} = (\theta - \Theta(\alpha))/\epsilon^{1/2}$, (C.2) becomes

$$\begin{aligned} A_m(\alpha,\epsilon) =& \epsilon^{-1/2}\int\int_0^{\epsilon^{-1}H_\epsilon(\theta)} \tilde{\psi}_m\left(\frac{\vec{\alpha}\cdot(y(\theta)-y(\Theta(\alpha)))}{\epsilon} + \hat{t}\cos(\theta-\alpha)\right) \\ &\times F(\theta,\epsilon\hat{t})\mathrm{d}\hat{t}\mathrm{d}\tilde{\theta},\quad \theta = \Theta(\alpha) + \epsilon^{1/2}\tilde{\theta},\ \alpha\in\Omega. \end{aligned} \tag{C.4}$$

Due to (7.10), we can integrate with respect to $\tilde{\theta}$ over any fixed neighborhood of 0,

$$\begin{aligned} &A_m(\alpha,\epsilon) \\ &= \epsilon^{-1/2}\int_{-\delta}^{\delta}\int_0^{\epsilon^{-1}H_\epsilon(\theta)} \tilde{\psi}_m\left(\frac{\vec{\alpha}\cdot y'(\Theta(\alpha))}{\epsilon^{1/2}}\tilde{\theta} + O(\tilde{\theta}^2) + \hat{t}\cos(\Theta(\alpha)-\alpha) + O(\epsilon^{1/2})\right) \\ &\quad\times\Big(F(\Theta(\alpha),0) + O(\epsilon^{1/2})\Big)\,\mathrm{d}\hat{t}\mathrm{d}\tilde{\theta} + (1+m^2)^{-1}O(\epsilon^{1/2}), \\ &\theta = \Theta(\alpha) + \epsilon^{1/2}\tilde{\theta},\quad \alpha\in\Omega, \end{aligned} \tag{C.5}$$

for some $\delta > 0$ sufficiently small. Here we have used that

$$\tilde{\psi}_m(t), \tilde{\psi}_m'(t) = (1+m^2)^{-1}O(t^{-2}),\ t\to\infty, \tag{C.6}$$

which follows from (7.7) and (7.9). Using (C.6) it is easy to see that the terms $O(\epsilon^{1/2})$ and $O(\tilde{\theta}^2)$ can be omitted from the argument of $\tilde{\psi}_m$ without changing the error term:

$$\begin{aligned} &A_m(\alpha,\epsilon) \\ &= \frac{F(\Theta(\alpha),0)}{\epsilon^{1/2}}\int_{-\delta}^{\delta}\int_0^{H_0(\epsilon^{-1/2}\Theta(\alpha)+\tilde{\theta})} \tilde{\psi}_m\left(\frac{\vec{\alpha}\cdot y'(\Theta(\alpha))}{\epsilon^{1/2}}\tilde{\theta} + \hat{t}\cos(\Theta(\alpha)-\alpha)\right)\mathrm{d}\hat{t}\mathrm{d}\tilde{\theta} \\ &\quad + (1+m^2)^{-1}O(\epsilon^{1/2}),\ \alpha\in\Omega. \end{aligned} \tag{C.7}$$

By (C.1), $\vec{\alpha}\cdot y'(\Theta(\alpha))$ is bounded away from zero on Ω. By the last equation in (7.8), $\int\tilde{\psi}_m(\hat{t})\mathrm{d}\hat{t} = 0$ for all m, so we can replace the lower limit of the inner integral in

(C.7) with any value independent of $\tilde{\theta}$. Again, we use here that the contribution to the integral with respect to $\tilde{\theta}$ of the domain outside $(-\delta, \delta)$ is of the same magnitude as the error term in (C.7). We choose the lower limit to be $H_0(\epsilon^{-1/2}\Theta(\alpha))$. Hence

$$|A_m(\alpha,\epsilon)| \le (1+m^2)^{-1}\left[O(\epsilon^{-1/2})\int_{-\delta}^{\delta}\frac{\left|H_0(s+\tilde{\theta})-H_0(s)\right|}{1+(\tilde{\theta}^2/\epsilon)}\mathrm{d}\tilde{\theta}+O(\epsilon^{1/2})\right], \tag{C.8}$$
$$s=\epsilon^{-1/2}\Theta(\alpha),\ \alpha\in\Omega.$$

Neglecting the $O(\epsilon^{1/2})$ term in (C.8) (the last term inside the brackets) leads to a term of magnitude $O(\epsilon^{1/2})$ in $f_\epsilon^{\mathrm{rec}}$. Accounting for (C.3) in a similar fashion, (7.13) and (C.8) imply

$$f_\epsilon^{\mathrm{rec}}(x) = O(\epsilon^{1/2})\int_{-\delta}^{\delta}\frac{g(\tilde{\theta},\epsilon)}{1+(\tilde{\theta}^2/\epsilon)}\mathrm{d}\tilde{\theta}+O(\epsilon^{1/2}), \tag{C.9}$$
$$g(\tilde{\theta},\epsilon) := \sum_{\alpha_k\in\Omega}\left|H_0(s_k+\tilde{\theta})-H_0(s_k)\right|,\ s_k := \epsilon^{-1/2}\Theta(\alpha_k).$$

If we use only the smoothness of H_0 (cf. (2.7)), the most we can say is that each term in the sum is $O(|\tilde{\theta}|^\gamma)$, so $g(\tilde{\theta},\epsilon) = O(\epsilon^{-1}|\tilde{\theta}|^\gamma)$. However, the structure of the sum allows us to exploit the assumption that the level sets of H_0 are not too dense, and this leads to a better estimate.

Define, similarly to (2.10),

$$\chi_{t_1,t_2}(t) := \begin{cases} 1, & t_1 \le t \le t_2 \text{ or } t_2 \le t \le t_1, \\ 0, & \text{otherwise.}\end{cases} \tag{C.10}$$

Clearly,

$$g(\tilde{\theta},\epsilon) = \sum_{\alpha_k\in\Omega}\int \chi_{H_0(s_k),H_0(s_k+\tilde{\theta})}(\hat{t})\mathrm{d}\hat{t} = \int N(\hat{t},\tilde{\theta},\epsilon)\mathrm{d}\hat{t}, \tag{C.11}$$

where $N(\hat{t},\tilde{\theta},\epsilon)$ is the number of $\alpha_k\in\Omega$ such that either $H_0(s_k)\le\hat{t}\le H_0(s_k+\tilde{\theta})$ or $H_0(s_k+\tilde{\theta})\le\hat{t}\le H_0(s_k)$. By the assumption in Lemma 7.1 about the level sets of H_0, N is finite for almost all $\hat{t}$. Our argument implies that the values of the index k counted by the function $N(\hat{t},\tilde{\theta},\epsilon)$ are such that the closed interval with the endpoints s_k and $s_k+\tilde{\theta}$ contains at least one $u_n\in H_0^{-1}(\hat{t})$. By assumption, the number of $u_n\in H_0^{-1}(\hat{t})$ on any interval of length $O(\epsilon^{-1/2})$ is $O(\epsilon^{-1/2})$ uniformly in $\hat{t}$ for almost all $\hat{t}$. Fix any n. By (C.1) and the definition of s_k in (C.9), there are no more than $1+O(\epsilon^{-1/2}|\tilde{\theta}|)$ values of k such that $|s_k-u_n|\le|\tilde{\theta}|$. Hence $N(\hat{t},\tilde{\theta},\epsilon) = O(\epsilon^{-1/2})(1+\epsilon^{-1/2}|\tilde{\theta}|)$. Using that the range of H_0 is bounded (cf. (2.7)), the integral with respect to $\hat{t}$ in (C.11) is over a compact set, so

$$g(\tilde{\theta},\epsilon) = O(\epsilon^{-1/2})(1+\epsilon^{-1/2}|\tilde{\theta}|). \tag{C.12}$$

Substituting (C.12) into (C.9), we finish the proof:

$$f_\epsilon^{\mathrm{rec}}(x) = O(1)\int_{-\delta}^{\delta}\frac{1+\epsilon^{-1/2}|\tilde{\theta}|}{1+(\tilde{\theta}^2/\epsilon)}\mathrm{d}\tilde{\theta}+O(\epsilon^{1/2}) = O(\epsilon^{1/2}\ln(1/\epsilon)). \tag{C.13}$$

The estimate in (C.13) is better than $O(\epsilon^{\gamma/2})$ if $\gamma<1$; cf. (3.33). The latter is the corresponding result in the original approach in subsection 3.4 (no line through x_0 with the unit normal in Ω_3 tangent to $\mathcal{S}$). This result can be rederived using the approach

in this section. Indeed, as mentioned above, (2.7) implies $g(\tilde{\theta},\epsilon) = O(\epsilon^{-1}|\tilde{\theta}|^{\gamma})$, and we compute, similarly to (C.13),

$$f_{\epsilon}^{\text{rec}}(x) = O(\epsilon^{-1/2}) \int_{-\delta}^{\delta} \frac{|\tilde{\theta}|^{\gamma}}{1+(\tilde{\theta}^2/\epsilon)} \mathrm{d}\tilde{\theta} + O(\epsilon^{1/2}) = O(\epsilon^{\gamma/2}),\ 0<\gamma<1. \tag{C.14}$$

Hence a truly novel mechanism (e.g., based on a consideration of the level sets of H_0) is needed to establish the faster decay rates in (7.14).

Appendix D. Example of a monotone, Hölder continuous function, which is nondifferentiable in a dense set. Set

$$H_0(s) = \sum_{n=0}^{\infty} \varphi(2^n s)/3^n,\ \varphi(s) := \lfloor s \rfloor + \{s\}^{\gamma}, \tag{D.1}$$

where $0<\gamma<1$. Obviously, the series above converges absolutely for any fixed s, and H_0 is strictly monotonically increasing.

Next we show that H_0 is locally Hölder continuous with exponent γ. We have

$$|\varphi(s_2)-\varphi(s_1)| \le c \max(|s_2-s_1|^{\gamma}, |s_2-s_1|),\ s_1,s_2 \ge 0, \tag{D.2}$$

for some c. The case $|s_2-s_1| \ge 1$ is obvious, so we assume $|s_2-s_1| \le 1$ and show that $\varphi(s_2)-\varphi(s_1) = O(|s_2-s_1|^{\gamma})$. Clearly, it suffices to consider the case $s_1 = n-1+r_1$, $s_2 = n+r_2$, where $0 \le r_{1,2} < 1$. We will show that

$$(n+r_2^{\gamma}) - (n-1+r_1^{\gamma}) \le (1+r_2-r_1)^{\gamma}. \tag{D.3}$$

The case $r_2 \ge r_1$ is obvious (and should not be considered anyway, because $s_2-s_1 \ge 1$ in this case), so we assume $r_2 = r_1 - h$, where $0 \le h \le r_1$. Then (D.3) becomes

$$(r_1-h)^{\gamma} + 1 - r_1^{\gamma} \le (1-h)^{\gamma}. \tag{D.4}$$

Differentiating the left-hand side we see that it is increasing as a function of $r_1 \in [h,1]$. Setting $r_1 = 1$ shows that the inequality holds.

Pick any $h>0$ and consider the difference

$$H_0(s+h) - H_0(s) = \left(\sum_{n \ge 0 : 2^n h < 1} + \sum_{n : 2^n h \ge 1} \right) \frac{\varphi(2^n(s+h)) - \varphi(2^n s)}{3^n} =: S_1 + S_2. \tag{D.5}$$

By (D.2),

$$|S_1| \le c h^{\gamma} \sum_{n \ge 0 : 2^n h < 1} 2^{\gamma n}/3^n \le c h^{\gamma},\ |S_2| \le ch \sum_{n : 2^n h \ge 1} 2^n/3^n \le ch, \tag{D.6}$$

which proves Hölder continuity. Here c denote various constants, which can be different in different places.

Finally we show that $H_0(s)$ is not Hölder continuous with any exponent $\gamma' > \gamma$ on any interval. Pick any $j,m \in \mathbb{N}$ and set $s = j2^{-m}$. Pick any $h \in (0, 2^{-m})$. Using that φ is increasing gives

$$\frac{H_0(s+h)-H_0(s)}{h^{\gamma'}} \ge \frac{\varphi(2^m(s+h)) - \varphi(2^m s)}{3^m h^{\gamma'}} = \frac{(j+(2^m h)^{\gamma}) - j}{3^m h^{\gamma'}} = c h^{\gamma-\gamma'}, \tag{D.7}$$

and the desired assertion follows because dyadic reals are dense in $\mathbb{R}$.

REFERENCES

[1] H. Abels, *Pseudodifferential and Singular Integral Operators: An Introduction with Applications*, De Gruyter, Berlin, 2012.

[2] L. M. Anovitz and D. R. Cole, *Characterization and analysis of porosity and pore structures*, Rev. Mineral. Geochem., 80 (2015), pp. 61–164, https://doi.org/10.2138/rmg.2015.80.04.

[3] K. Barański, *Dimension of the graphs of the Weierstrass-type functions*, in Fractal Geometry and Stochastics V, Progr. Probab. 70, C. Bandt, K. Falconer, and M. Zähle, eds., Birkhauser, Heidelberg, 2015, pp. 77–91, https://doi.org/10.1007/978-3-319-18660-3_5.

[4] M. V. Berry and Z. V. Lewis, *On the Weierstrass-Mandelbrot fractal function*, Proc. A, 370 (1980), pp. 459–484, https://doi.org/10.1098/rspa.1980.0044.

[5] T. Blu, P. Thévenaz, and M. Unser, *Complete parameterization of piecewise-Polynomial interpolation kernels*, IEEE Trans. Image Process., 12 (2003), pp. 1297–1309.

[6] F. M. Borodich and D. A. Onishchenko, *Similarity and fractality in the modelling of roughness by a multilevel profile with hierarchical structure*, Internat. J. Solids Struct. 36 (1999), pp. 2585–2612, https://doi.org/10.1016/S0020-7683(98)00116-4.

[7] E. Cherkaev, A. H. Khan, and A. C. Tripp, *Fracture surface characterization through x-ray tomography*, in Twenty-Fifth Workshop on Geothermal Reservoir Engineering, Stanford Geothermal Program, Stanford, CA, 2000, SGP-TR–165.

[8] O. Dovgoshey, O. Martio, V. Ryazanov, and M. Vuorinen, *The Cantor function*, Expo. Math., 24 (2006), pp. 1–37, https://doi.org/10.1016/j.exmath.2005.05.002.

[9] C. L. Epstein, *Introduction to the Mathematics of Medical Imaging*, 2nd ed., SIAM, Philadelphia, 2008.

[10] A. Faridani, *Sampling theory and parallel-beam tomography*, in Sampling, Wavelets, and Tomography, Appl. Numer. Harmon. Anal. 63, Birkhauser Boston, Boston, MA, 2004, pp. 225–254.

[11] A. Faridani, K. Buglione, P. Huabsomboon, O. Iancu, and J. McGrath, *Introduction to local tomography*, in Radon Transforms and Tomography, Contemp. Math., 278, American Mathematical Society, Providence, RI, 2001, pp. 29–47.

[12] I. M. Gelfand, M. I. Graev, and N. Y. Vilenkin, *Generalized Functions. Volume 5: Integral Geometry and Representation Theory*, Academic Press, New York, 1966.

[13] S. I. Gonchar, *Convergence of computational algorithms for recovering discontinuous functions from the Radon transform*, Russian Math. Surveys, 41 (1986), pp. 205–206.

[14] J.-F. Gouyet, M. Rosso, and B. Sapoval, *Fractal surfaces and interfaces*, in Fractals and Disordered Systems, 2nd rev ed., A. Bunde and S. Havlin, eds., Springer, Berlin, 1996, pp. 263–302.

[15] B. Hahn and A. K. Louis, *Reconstruction in the three-dimensional parallel scanning geometry with application in synchrotron-based x-ray tomography*, Inverse Problems, 28 (2012), 045013.

[16] S. Helgason, *The Radon Transform*, 2nd ed., Birkhauser, Boston, 1999.

[17] A. K. Jain and S. Ansari, *Radon transform theory for random fields and optimum image reconstruction from noisy projections*, in ICASSP, IEEE International Conference on Acoustic, Speech and Signal Processing, IEEE, New York, 1984, pp. 495–498, https://doi.org/10.1109/icassp.1984.1172341.

[18] A. Katsevich, *A local approach to resolution analysis of image reconstruction in tomography*, SIAM J. Appl. Math., 77 (2017), pp. 1706–1732.

[19] A. Katsevich, *Analysis of reconstruction from discrete Radon transform data in $\mathbb{R}^3$ when the function has jump discontinuities*, SIAM J. Appl. Math., 79 (2019), pp. 1607–1626.

[20] A. Katsevich, *Analysis of resolution of tomographic-type reconstruction from discrete data for a class of distributions*, Inverse Problems, 36 (2020), 124008, https://doi.org/10.1088/1361-6420/abb2fb.

[21] A. Katsevich, *Resolution analysis of inverting the generalized Radon transform from discrete data in $\mathbb{R}^3$*, SIAM J. Math. Anal., 52 (2020), pp. 3990–4021.

[22] A. Katsevich, *Resolution analysis of inverting the generalized N-dimensional Radon transform in $\mathbb{R}^n$ from discrete data*, J. Fourier. Anal. Appl., 29 (2023), 6.

[23] R. G. Keys, *Cubic convolution interpolation for digital image processing*, IEEE Trans. Acoust. Speech Signal Process., 29 (1981), pp. 1153–1160, https://doi.org/10.1109.TASSP.1981.1163711.

[24] A. N. Kolmogorov and S. V. Fomin, *Introductory Real Analysis*, Dover Publications, New York, 1975.

[25] X. Li, M. Luo, and J. Liu, *Fractal characteristics based on different statistical objects of process-based digital rock models*, J. Petrol. Sci. Eng., 179 (2019), pp. 19–30, https://doi.org/10.1016/j.petrol.2019.03.068.

[26] A. K. Louis, *Exact cone beam reconstruction formulae for functions and their gradients for spherical and flat detectors*, Inverse Problems, 32 (2016), 115005.
[27] J. M. Médina, *On the Radon Transform of Stationary Random Fields*, preprint, hal-02915444, 2020.
[28] F. Monard and P. Stefanov, *Sampling the X-Ray Transform on Simple Surfaces*, preprint, arXiv:2110.05761, 2021, http://arxiv.org/abs/2110.05761
[29] F. Natterer, *Sampling in fan beam tomography*, SIAM J. Appl. Math., 53 (1993), pp. 358–380.
[30] F. Natterer, *The Mathematics of Computerized Tomography*, Classics Appl. Math. 32, SIAM, Philadelphia, 2001.
[31] Y. Pachepsky, J. W. Crawford, and W. J. Rawls, eds., *Fractals in Soil Science*, Elsevier, Amsterdam, 2000.
[32] V. P. Palamodov, *Some mathematical aspects of 3D X-ray tomography*, in Proceedings of the Conference: Tomography, impedance imaging, and integral geometry (South Hadley, MA, 1993), Lect. Appl. Math. 30, American Mathematical Society, Providence, RI, 1994, pp. 199–210.
[33] V. P. Palamodov, *Localization of harmonic decomposition of the Radon transform*, Inverse Problems, 11 (1995), pp. 1025–1030.
[34] D. A. Popov, *On convergence of a class of algorithms for the inversion of the numerical Radon transform*, in Mathematical Problems of Tomography, Transl. Math. Monogr. 81, American Mathematical Society, Providence, RI, 1990, pp. 7–65.
[35] D. A. Popov, *Reconstruction of characteristic functions in two-dimensional Radon tomography*, Russian Math. Surveys, 53 (1998), pp. 109–193.
[36] W. L. Power and T. E. Tullis, *Euclidean and fractal models for the description of rock surface roughness*, J. Geophys. Res., 96 (1991), pp. 415–424.
[37] A. Ramm and A. Katsevich, *The Radon Transform and Local Tomography*, CRC Press, Boca Raton, Florida, 1996.
[38] F. Renard, *Three-dimensional roughness of stylolites in limestones*, J. Geophys. Res., 109 (2004), pp. 1–12, https://doi.org/10.1029/2003jb002555.
[39] F. Rezakhanlou, *The packing measure of the graphs and level sets of certain continuous functions*, Math. Proc. Cambridge Philos. Soc., 104 (1988), pp. 347–360.
[40] J. Sanz, E. Hinkle, and A. Jain, *Radon transform theory for random fields and optimum image reconstruction from noisy projections*, in Radon and Projection Transform-Based Computer Vision, Springer Ser. Inform. Sci. 16, Springer, Berlin, 1988.
[41] P. Stefanov, *Semiclassical sampling and discretization of certain linear inverse problems*, SIAM J. Math. Anal., 52 (2020), pp. 5554–5597.
[42] J. Thim, *Generating Continuous Nowhere Differentiable Functions*, Master's, Lulea University of Technology, Lulea, Sweden, 2003.
[43] H. Yu, *Weak tangent and level sets of Takagi functions*, Monatsh. Math., 192 (2020), pp. 249–264, https://doi.org/10.1007/s00605-020-01377-9.
[44] L. Zhu, C. Zhang, C. Zhang, X. Zhou, Z. Zhang, X. Nie, W. Liu, and B. Zhu, *Challenges and prospects of digital core-reconstruction research*, Geofluids, 2019 (2019), https://doi.org/10.1155/2019/7814180.